doi.org/10.1002/cbdv.202301089 Research Article CHEMISTRY & BIODIVERSITY

www.cb.wiley.com

Synthesis and Anticancer Activity of Novel Derivatives of α,β-Unsaturated Ketones Based on Oleanolic Acid: *in Vitro* and *in Silico* Studies against Prostate Cancer Cells

Halil Şenol,*[a] Mansour Ghaffari-Moghaddam,*[a, b] Şeyma Bulut,[c, d] Fahri Akbaş,[d] Aytekin Köse,[e] and Gülaçtı Topçu[f]

Herein, new derivatives of α,β-unsaturated ketones based on oleanolic acid (**4a**–**i**) were designed, synthesized, characterized, and tested against human prostate cancer (PC3). According to the *in vitro* cytotoxic study, title compounds (**4a**–**i**) showed significantly lower toxicity toward healthy cells (HUVEC) in comparison with the reference drug doxorubicin. The compounds with the lowest IC_{50} values on PC3 cell lines were **4b** (7.785 μM), **4c** (8.869 μM), and **4e** (8.765 μM). The results of the ADME calculations showed that the drug-likeness parameters were within the defined ranges according to Lipinski's and Jorgensen's rules. For the most potent compounds **4b**, **4c**, and **4e**, a molecular docking analysis using the induced fit docking (IFD) protocol was performed against three protein targets (PARP, PI3K, and mTOR). Based on the IFD scores, compound **4b** had the highest calculated affinity for PARP1, while compound **4c** had higher affinities for mTOR and PI3K. The MM-GBSA calculations showed that the most potent compounds had high binding affinities and formed stable complexes with the protein targets. Finally, a 50 ns molecular dynamics simulation was performed to study the behavior of protein target complexes under *in silico* physiological conditions.

Introduction

Prostate cancer (PCa) is nowadays one of the most common cancers in men.[1] The prostate gland is an androgen-dependent organ, and PCa is originally dependent on androgen receptor for growth and survival.[2] Therefore, inhibiting the enzymes that play an important role in the biosynthesis of androgen is a promising approach for the treatment of prostate cancer.[3] Although, androgen receptor blockers (such as enzalutamide and apalutamide) are clinically used to treat most prostate cancer patients, most treated patients will eventually develop castrate resistance within two to three years.[4] Over the past decades, the role of androgen-receptor signaling has consistently remained important in PCa therapy.[5] However, recent studies have highlighted the contribution of DNA-damage response (DDR) pathways in the progression of a considerable number of PCa.[6] Poly (adenosine diphosphate-ribose) polymerase-1 (PARP-1) is a multifunctional nuclear enzyme that regulates chromatin structure and transcription through its multiple domains.[7] A mutation of the DDR gene causes cancer cells depending on PARP-1 for DNA repair. When PARP-1 is inhibited, these cells undergo death. This process, also known as synthetic lethality, offers the use of PARP inhibitors as a successful therapy strategy.[6] The PI3K-AKT-mTOR signaling pathway is recognized as a prevalent pathway characterized by abnormal activation in tumor cells. It plays a pivotal role in various crucial functions, including tumor cell growth, proliferation, migration, invasion, and the promotion of tumor angiogenesis.[8] Phosphoinositide 3-kinases (PI3Ks) are a crucial group of lipid kinases that are involved in the regulation of various cellular processes, including anabolic and catabolic activities. Their main function is to catalyze the phosphorylation of the 3′-OH group of phosphoinositides and phosphatidylinositol molecules.[9] The PI3K signaling pathway is crucial for cellular functions and is involved in various diseases, such as cancer. Developing effective PI3K inhibitors is critical in the design of anti-tumor drugs.[10] mTOR (the Mammalian target of rapamycin), belongs to the family of PIKK (Phosphatidylinositol 3-kinase-related kinases). It can be activated by Akt (Protein kinase B), leading to the stimulation of new protein synthesis and cell proliferation. mTOR forms two different protein complexes known as mTORC1 and mTORC2 by binding to different proteins with unique structural properties.[11] The overactivation or overexpression of mTOR plays a crucial role in

[a] *Dr. H. Şenol, Dr. M. Ghaffari-Moghaddam*
Bezmialem Vakif University, Faculty of Pharmacy, Department of Pharmaceutical Chemistry, 34093 Fatih, Istanbul, Türkiye
E-mail: hsenol@bezmialem.edu.tr
mansghaffari@uoz.ac.ir

[b] *Dr. M. Ghaffari-Moghaddam*
University of Zabol, Faculty of Science, Department of Chemistry, Zabol, 98615-538 Iran

[c] *Ş. Bulut*
Bezmialem Vakif University, Institute of Health Sciences, Department of Biotechnology, 34093 Fatih, Istanbul, Türkiye

[d] *Ş. Bulut, Dr. F. Akbaş*
Bezmialem Vakif University, Faculty of Medicine, Department of Medical Biology, 34093 Fatih, Istanbul, Türkiye

[e] *Dr. A. Köse*
Aksaray University, Faculty of Science and Letters, Department of Chemistry, 68100 Aksaray, Türkiye

[f] *Dr. G. Topçu*
Bezmialem Vakif University, Faculty of Pharmacy, Department of Pharmacognosy & Phytochemistry Chemistry, 34093 Fatih, Istanbul, Türkiye

Supporting information for this article is available on the WWW under https://doi.org/10.1002/cbdv.202301089

the progression of various cancers. As a result, mTOR is a critical pharmacological target for cancer treatment, and numerous mTOR inhibitors have been extensively studied in clinical trials, with some even gaining approval for marketing purposes.[12]

Oleanolic acid (3β-hydroxyolean-12-en-28-oic acid, OA) is a natural pentacyclic triterpenoid with the molecular formula $C_{30}H_{48}O_3$. It is commonly found in the *Oleaceae* family of plants such as *Olea* europaea,[13] OA and its derivatives show several pharmacological activities, such as anti-oxidant, anti-inflammatory, anti-HIV, anti-cholinesterase, and anti-cancer properties.[14] Particularly, the anti-cancer properties of OA are its most important function because they can affect numerous cancer pathways.[15] However, OA has a number of drawbacks, including poor solubility in water, poor bioavailability, and minimal bioactivity, which limit its potential therapeutic applications.[16] To overcome this problem, various methods, such as chemical modification, have been implemented to increase its water solubility and pharmacological activity.[15]

Molecular docking is an *in silico* technique for identifying the proper binding orientation of a ligand-receptor complex.[17] The goals of molecular docking are (i) to identify the mode of binding of a ligand to a receptor that results in the lowest energy score and (ii) to determine an estimate of the affinity of the interaction between ligand and receptor. This useful information can be utilized to develop novel drugs and to understand how ligand-receptor interactions work.[18] Molecular docking is usually classified into three classes: induced fit docking (IFD), ensemble docking, and lock and key docking.[19] Among them, the IFD approach stands out since it provides a more precise depiction of the spatial conformation of the receptor in the presence of ligands. IFD is more suitable compared to rigid receptor docking because of its improved capability, which allows more accurate evaluation of the resulting complex.[20]

Molecular dynamics (MD) is a computer simulation technique to understand the dynamics and temporal evolution of molecules.[21] MD simulations are carried out by simulating the intra- and inter-molecular interactions using classical mechanics models.[22] These simulations can provide various biomolecular processes, including conformational change, ligand binding, and protein folding, which display the positions of all the atoms at femtosecond temporal resolution. At an atomic level, the MD simulations also predict how biomolecules will react to perturbations such as mutation, phosphorylation, protonation, or the addition or removal of a ligand.[23]

In our preliminary molecular docking studies, we noticed an interesting observation regarding the phenyl ring and ester group of α,β-unsaturated ketones based on oleanolic acid. Specifically, we found that incorporating certain groups such as $-NO_2$, $-CF_3$, –CN, and –OMe on the phenyl ring and using a MOM (methoxymethyl) ester at C-28 of oleanolic acid significantly improved the interaction of these compounds with the target enzymes. Therefore, in the present research work, we explored the synthesis and characterization of a new class of derivatives of α,β-unsaturated ketones based on oleanolic acid (**4a–i**). The *in vitro* cytotoxicity evaluation of all title compounds and OA, as well as the reference drug doxorubicin (Dox), was performed using the MTT assay method against human prostate cancer (PC3) and human umbilical vein endothelial cells (HUVEC) as a healthy control. Molecular docking analysis was carried out to study how the compounds interacted with receptors. Molecular dynamics simulation was also used to investigate the stability of ligand-receptor complexes. Furthermore, theoretical computational ADME analysis was used to predict the pharmacokinetic properties of the compounds.

Results and Discussion

Synthesis and characterization

The synthesis of the title compounds was carried out in three steps, starting from natural product oleanolic acid (Scheme 1), as follows: The derivative of methoxymethyl 3β-hydroxyolean-12-en-28-oate (**2**) was synthesized from oleanolic acid (**1**) using bromomethyl methyl ether (MOMBr) by the esterification reaction in the presence of NaH at 0 °C.[14f] Then the hydroxy group was oxidized by pyridinium chlorochromate (PCC) in dichloromethane at room temperature to give the derivative of methoxymethyl 3-oxo-olean-12-en-28-oate (**3**).[14c] To obtain the Claisen-Schmidt products (**4a–i**), compound **3** was condensed with different aromatic aldehydes in the presence of a basic catalyst (potassium ethoxide) at room temperature. All the compounds were synthesized in good yield. The sharp melting points obtained demonstrated that the synthesized compounds are pure enough. The chemical structures of the synthesized compounds were elucidated using ^{1}H-NMR, ^{13}C APT NMR, COSY, HSQC, HMBC, ^{19}F NMR, FT-IR, and HR-ESI-MS spectroscopic techniques, and the resulting spectral data were provided in the experimental section.

In the ^{1}H-NMR spectrum of compound **2**, for the C-28 carboxylic acid MOM ester, two doublet signals, belonging to the CH_2 protons of the MOM group, resonated at 5.25 and 5.18 ppm. The CH_2 carbon of the MOM group resonated at 90.45 ppm in the ^{13}C APT NMR spectrum. Furthermore, the methoxy of the MOM group resonated at 3.47 and 57.60 ppm in the ^{1}H and ^{13}C APT NMR spectra, respectively. In compound **2**, the ester carbonyl resonated at 177.24 ppm, whereas the carboxylic acid carbon resonated at 184 ppm in oleanolic acid.[14c–d,f] In the ^{13}C APT NMR spectrum, compound **3** shows a signal at 217.57 ppm, corresponding to the C-3 keto carbonyl. In compound **2**, the H-3 proton resonated at 3.22 ppm as a doublet of doublets in the ^{1}H-NMR spectrum, whereas this signal was lost in compound **3** due to the formation of a ketone. Furthermore, the C-3 carbon of compound **2** shifted from 79 ppm to 217.57 ppm in the ^{13}C APT NMR spectrum of compound **3**. In conclusion, the synthesis of compounds **2** and **3** was confirmed by NMR spectroscopy.

The α-β unsaturated system of the compounds **4**(**a–i**), C-3 ketone carbonyl signal shifted from 217 ppm to 206–207 ppm in the ^{13}C APT NMR, due to carbonyl conjugation. The β proton of compounds **4**(**a–i**) resonated as a singlet in the ^{1}H-NMR spectrum in the range of 7–8 ppm. All compounds (**2–4**) have seven CH_3 singlet signals in the aliphatic region (1.1–0.6 ppm).

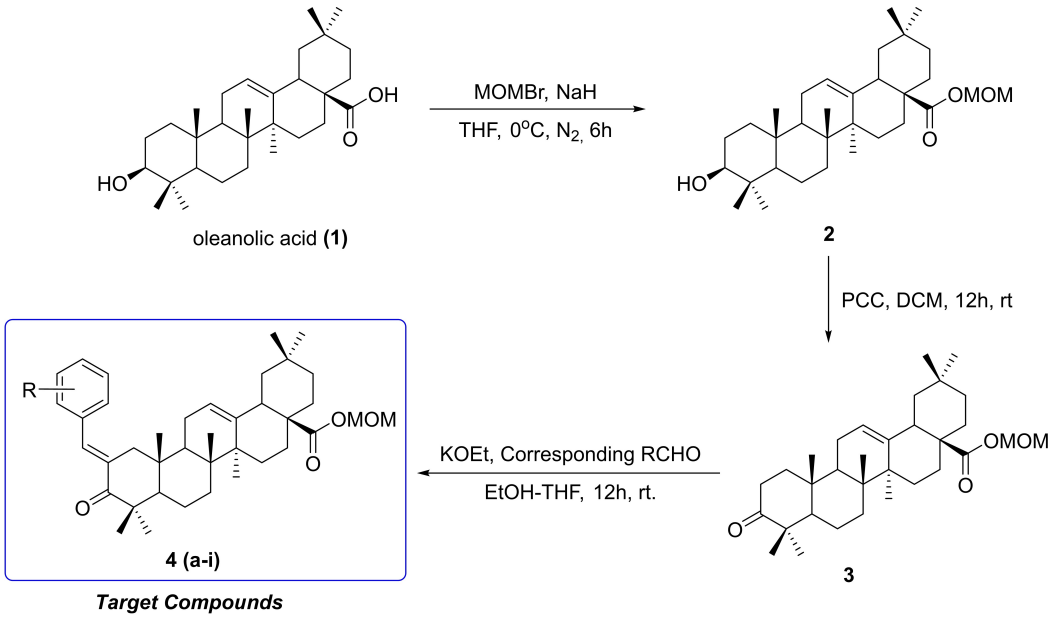

R= a: 2-NO_2, **b:** 3-NO_2, **c:** 4-NO_2, **d:** 3-CF_3, **e:** 4-CF_3, **f:** 3,5-bisCF_3, **g:** 4-CN, **h:** 2-OMe, **i:** 4-OMe

Scheme 1. Schematic representation of the synthetic routes for the title compounds **4** (**a**–**i**).

In the ^{13}C APT NMR spectrum of compound **4g**, the carbon of CN resonated at 118.67 ppm. The OMe group of compounds **4h** and **4i**, resonated at 3.76 and 3.74 ppm in ^{1}H and their carbons resonated at 55.50 and 55.30 ppm in ^{13}C APT NMR, respectively.

The CF_3 groups of compound **4f** were observed at −62.97 ppm in the ^{19}F NMR spectrum as a singlet. In the ^{13}C APT NMR spectrum the CF_3 carbon resonated around 125 ppm as a quartet with a coupling constant of 272. The fluorine atoms of the CF_3 group split the carbon into a quartet with 33 over two bonds (ipso carbon), while the carbons at three bonds (CF_3 *ortho* position) and four bonds (CF_3 *meta* position) were split into quartets with coupling constants of 4 and 3.8, respectively. The detailed ^{13}C APT NMR analysis of **4e** is given in Figure 1.

Table 1. The IC_{50} values (μM) and selectivity index of cell lines treated with title compounds.

	IC_{50} [μM]		Selectivity index (SI)
Compounds	HUVEC	PC3	HUVEC/PC3
4a	52.19 ± 1.13	17.08 ± 0.18	3.05
4b	**58.23 ± 1.92**	**7.785 ± 0.08**	**7.48**
4c	**84.58 ± 2.01**	**8.869 ± 0.09**	**9.54**
4d	46.85 ± 1.18	9.903 ± 0.11	4.73
4e	**69.90 ± 1.25**	**8.765 ± 0.10**	**7.97**
4f	53.25 ± 1.48	17.08 ± 0.15	3.11
4g	52.28 ± 1.35	13.92 ± 0.16	3.75
4h	56.88 ± 1.32	10.90 ± 0.15	5.22
4i	60.30 ± 1.66	17.62 ± 0.24	3.42
Oleanolic acid	41.47 ± 1.37	9.93 ± 0.13	4.17
Doxorubicin	9.06 ± 0.11	5.33 ± 0.61	1.70

In vitro cytotoxicity studies

As a result of the fact that patients with metastatic cancers require selective anticancer drugs, the selective cytotoxicity of the title compounds (**4a**–**i**) was performed against human prostate cancer (PC3) and human umbilical vein endothelial cells (HUVEC) using the MTT assay.[24] The results, displayed as IC_{50} (μM) and selectivity index (SI) are listed in Table 1. Here, doxorubicin was used as a positive control (reference drug) to compare the effects of experimental compounds. The selectivity index shows the relative selectivity of a particular compound towards cancer cells compared to normal cells. A higher selectivity index value suggests a greater degree of selectivity.[25] According to Table 1, the IC_{50} values for the title compounds, OA, and doxorubicin against healthy cells (HUVEC) vary from 9.06 to 84.58 μM. Among them, compound **4c**, with an IC_{50} of 84.58 μM, displayed the lowest cytotoxicity against HUVEC cells. Other compounds that had the lowest cytotoxicity when tested on healthy cells (HUVEC) were **4e**, **4i**, and **4b**, with IC_{50} values of 69.90, 60.30, and 58.23 μM, respectively. Compared to the IC_{50} value of 9.06 μM for the reference drug doxorubicin, the title compounds were significantly less toxic to healthy cells than doxorubicin.

The IC_{50} values of the title compounds, OA, and doxorubicin on PC3 cancer cells lie in the range of 5.33 to 17.62 μM. Among the title compounds, compounds **4b** (7.785 μM), **4c** (8.869 μM), and **4e** (8.765 μM) showed the lowest IC_{50} values. According to the selectivity index results ranging from 1.7 to 9.54, title compounds were found to be more selective against PC3 cancer cells compared to the reference drug doxorubicin.

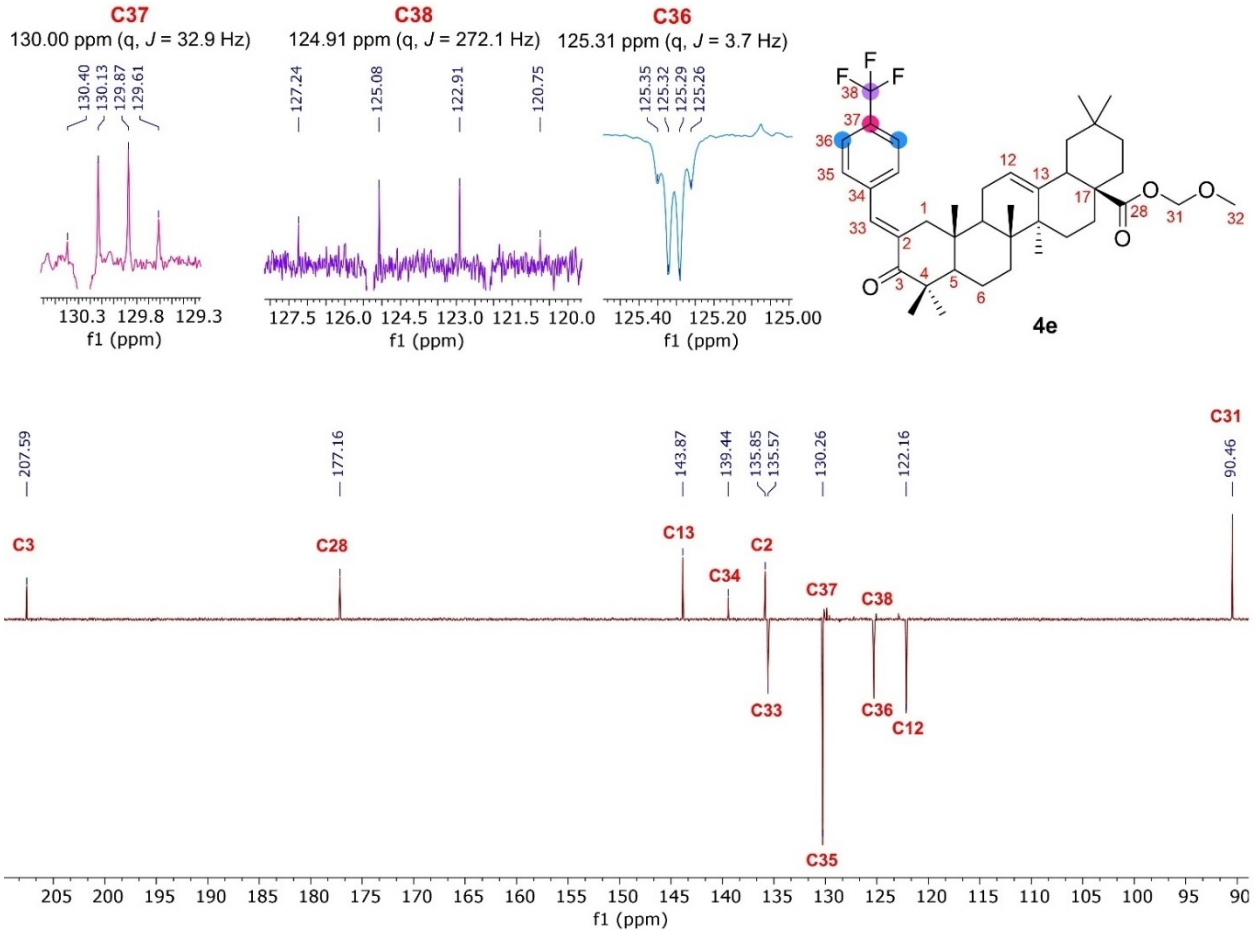

Figure 1. The detailed ^{13}C APT NMR spectrum and peak splitting's of compound **4e**.

Although the reference drug doxorubicin exhibited the lowest IC_{50} value (5.33 μM) against PC3 cells, its selectivity index (1.70) was very low. Therefore, these results suggested that compounds **4c**, **4e**, and **4b** with the highest selectivity index (9.54, 7.97, and 7.48) could be considered promising, selective, and potent candidates for future anticancer drug discovery and research against human prostate cancer.

Structure-activity relationship (SAR)

A structure-activity relationship (SAR) study was carried out on the title compounds (**4a**–**i**) to find the influence of various factors on their biological activity. The SAR study was mainly involved in determining how the nature, number, and position of substituents attached to the phenyl ring influence the potency of compounds against particular PC3 cell lines. Compounds **4a**, **4b**, and **4c** containing NO_2 at the *ortho*-, *meta*-, and p*ara*- positions of the phenyl ring had different IC_{50} values, indicating that the position of the nitro group on the phenyl ring influences activity. Compounds **4b** and **4c** with NO_2 at the *meta*- and *para*- positions of the phenyl ring had the highest potency against PC3 cell lines. In comparison with OA, compound **4d** with a *meta*-CF_3 on the phenyl ring had a slightly lower IC_{50} value, and compound **4e** with a *para*-CF_3 on the phenyl ring had a lower IC_{50} value, suggesting enhanced potency. Compound **4f**, which contains 3,5-bis CF_3 substitutions on the phenyl ring, had a higher IC_{50} value than OA and the same IC_{50} value as compound **4a**, indicating that more substitutions do not result in significant improvement. Compound **4g** containing a *para*-CN group on the phenyl ring had a higher IC_{50} value compared to the reference drug DOX and OA, indicating reduced potency. Compounds **4h** and **4i** having a methoxy group at the *ortho*- and *para*- positions on the phenyl ring had a higher IC_{50} value than the reference drug DOX and OA; however, compound **4i** had almost the same IC_{50} value as compound **4a**, indicating that electron donating substituents reduced potency. In summary, the SAR trends observed in the title compounds suggest that the position and nature of substituents on the phenyl ring can affect biological activity. Compounds containing specific substitutions, such as CF_3 and NO_2, at positions *meta*- and *para*- on the phenyl ring, showed higher potency. The SAR study of newly synthesized compounds tested for their anticancer activity is shown in Scheme 2.

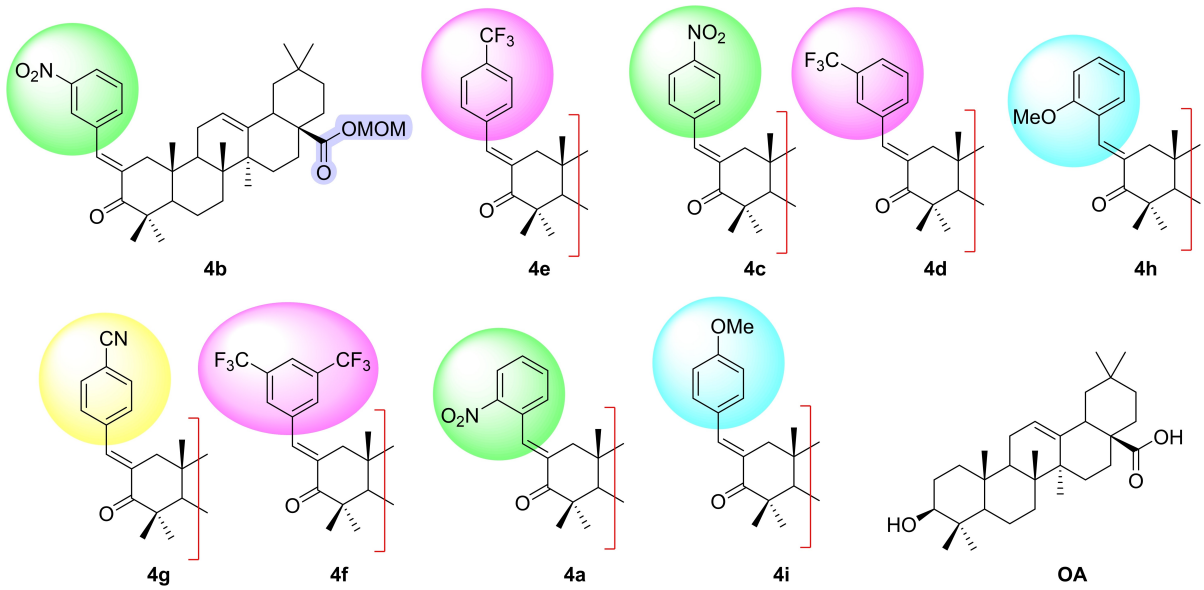

Scheme 2. The structure-activity relationship (SAR) study of newly synthesized compounds evaluated for their anticancer activity.

Molecular docking studies and prime MM-GBSA Δ G binding free energy calculations

Molecular docking is used to better understand the types of interactions between the active sites of proteins and ligands.[26] In the standard molecular docking approach, the ligands are only flexible molecules, while the protein is typically considered rigid.[27] In our preliminary experiments, we conducted molecular docking using this approach for our molecules. However, due to the large size of our ligands, they could not fit within the active site. Thus, these findings strongly suggest an induced fit docking (IFD) protocol in which both the ligands and the protein are flexible. This method could clarify the remarkable affinity exhibited by our compounds. In this study, the *in vitro* most active and most selective compounds (**4b**, **4c**, and **4e**) were selected and successfully docked into the active sites of human PARP1 (PDB ID: 5WS1), mTOR (PDB ID: 4JT5), and PI3K (PDB ID: 4L23) protein targets by means of an IFD protocol.

Using molecular mechanics-generalized born surface area (MM-GBSA) calculations to find the free binding energy is an excellent way to confirm the predicted potential affinity of a ligand for its protein target.[28] The more negative MM-GBSA ΔG binding free energy values show greater binding free energy, indicating more efficient interaction and a more stable ligand-receptor complex.[29] In this study, prime MM-GBSA ΔG binding free energy values were computed to analyze the binding modes of the most active compounds (**4b**, **4c**, and **4e**) into the selected protein targets to determine the binding stability between ligand and receptor complexes of docked molecules through calculating the free binding energy. The IFD docking scores (kcal/mol) and MM-GBSA ΔG binding free energies were used to determine the binding properties and binding affinity of molecules. The IFD docking scores and MM-GBSA ΔG Binding free energies of the most active compounds are given in Table 2.

For protein target PARP1, compounds **4b**, **4c**, and **4e** had the MM-GBSA ΔG free binding energies of −68.43, −76.70, and −61.36 kcal/mol, respectively. Compound **4c**, with the highest negative MM-GBSA ΔG free binding energy, suggests the strongest binding affinity and the most stable ligand-receptor complex for this protein target (Table 2). For protein target mTOR, the MM-GBSA ΔG free binding energies of the compounds were as follows: compound **4b** with a value of −64.75 kcal/mol, compound **4c** with a value of −63.74 kcal/mol, and compound **4e** with a value of −75.55 kcal/mol. Among these compounds, compound **4e** exhibits the most negative MM-GBSA ΔG free binding energy value, indicating the strongest binding affinity, the most efficient interactions,

Table 2. The IFD docking scores (kcal/mol) and MM-GBSA ΔG binding free energies (kcal/mol) of the most active compounds against target proteins.

	PARP1		mTOR		PI3K	
	IFD	MMGBSA	IFD	MMGBSA	IFD	MMGBSA
4b	−10.505	−68.43	−9.146	−64.75	−8.964	−86.23
4c	−9.496	−76.70	−10.291	−63.74	−10.897	−72.80
4e	−7.960	−61.36	−10.195	−75.55	−9.330	−63.95

and the most stable complex for protein target mTOR (Table 2). For protein target PI3K, the MM-GBSA ΔG free binding energies for three compounds were as follows: compound **4b** had a value of −86.23 kcal/mol, compound **4c** had a value of −72.80 kcal/mol, and compound **4e** had a value of −63.95 kcal/mol. Comparing the values, compound **4b** demonstrates the most negative MM-GBSA ΔG free binding energy value, suggesting the strongest binding affinity and the most efficient interaction for protein target PI3K (Table 2).

Molecular docking analysis on PARP1 protein target

For the protein target PARP1, compounds **4b**, **4c**, and **4e** exhibited IFD docking scores of −10.505, −9.496, and −7.960 kcal/mol, respectively. If the IFD score was lower, then the ligand and the protein target were expected to have higher binding affinity for each other. Therefore, compound **4b** demonstrated the highest predicted affinity for PARP1 among the three compounds. Molecular docking 2D and 3D ligand-protein interactions of the **4b-PARP1** complex are given in Figure 2 as combined. Moreover, molecular docking 2D and 3D ligan-protein interactions of **4c-PARP1** and **4e-PARP1** complexes and their evaluations were given in the supporting material. As depicted in Figure 2, compound **4b** shows two hydrogen bond interactions between the carbonyl group of the ester moiety and the Asn-767 with a distance of 2.76 Å, and the oxygen atom of the nitro group and the Gly-863 with a distance of 3.03 Å, and a cation-π interaction between the nitro group and the His-862.

Molecular docking analysis on mTOR protein target

For the protein target mTOR, the IFD scores for compounds **4b**, **4c**, and **4e** were −9.146, −10.291, and −10.195 kcal/mol, respectively. Both compounds **4c** and **4e** displayed slightly stronger predicted affinities compared to **4b**. This suggests that they may have more favourable binding interactions with the mTOR protein target. Molecular docking 2D and 3D ligand-protein interactions of the **4b-mTOR** complex were given in Figure 3 as combined. Moreover, molecular docking 2D and 3D ligan-protein interactions of the **4c-mTOR** and **4e-mTOR** complexes and their evaluations are given in the supporting material. As depicted in Figure 3, compound **4b** exhibits hydrogen bonds between the oxygen atom of the MOM group and the Ser-2165 with a distance of 3.07 Å, the carbonyl group of the ketone and the Val-2240 with a distance of 2.97 Å, and the oxygen atom of the nitro group and the Asp-2357 with a distance of 2.99 Å. It also forms two cation-π interactions between the nitrogen atom of nitro group and the residues Tyr-2225 and Asp-2357 with distances of 4.89 and 4.91 Å, respectively.

Molecular docking analysis on PI3K protein target

For the protein target PI3K, compound **4b** had an IFD score of −8.964 kcal/mol, while compounds **4c** and **4e** had IFD scores of −10.897 and −9.330 kcal/mol, respectively. In this case, compound **4c** showed the highest predicted affinity, indicating it may have stronger binding interactions with the protein target compared to the other compounds. Molecular docking 2D and 3D ligand-protein interactions of the **4c-PI3K** complex are given in Figure 4 as combined. Moreover, molecular docking 2D and 3D ligand-protein interactions of **4b-PI3K** and **4e-PI3K** complexes and their evaluations were given in the supporting material.

As shown in Figure 4, compound **4c** shows three hydrogen bonds, including interactions between the carbonyl group of the ester moiety and Thr-856 with a distance of 2.93 Å, the carbonyl group of the ketone moiety and Lys-802 with a distance of 3.66 Å. It also forms a π-π interaction between the phenyl ring and Tyr-836 with a distance of 3.37 Å, and a cation-π interaction between the nitrogen atom of the nitro group and Tyr-836 with a distance of 5.00 Å.

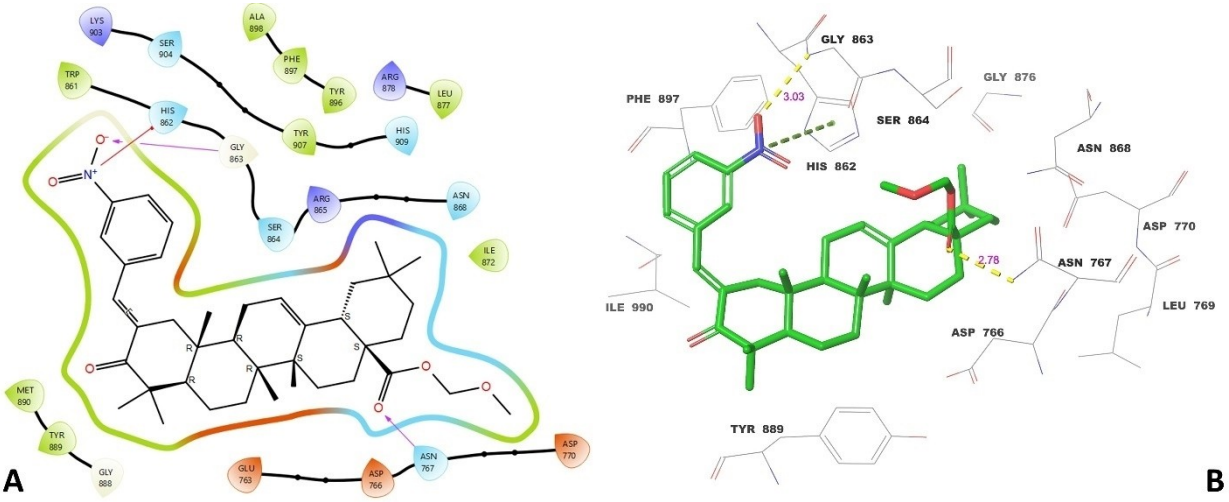

Figure 2. Molecular docking 2D (A) and 3D (B) ligand-protein interactions of **4b-PARP1** complex.

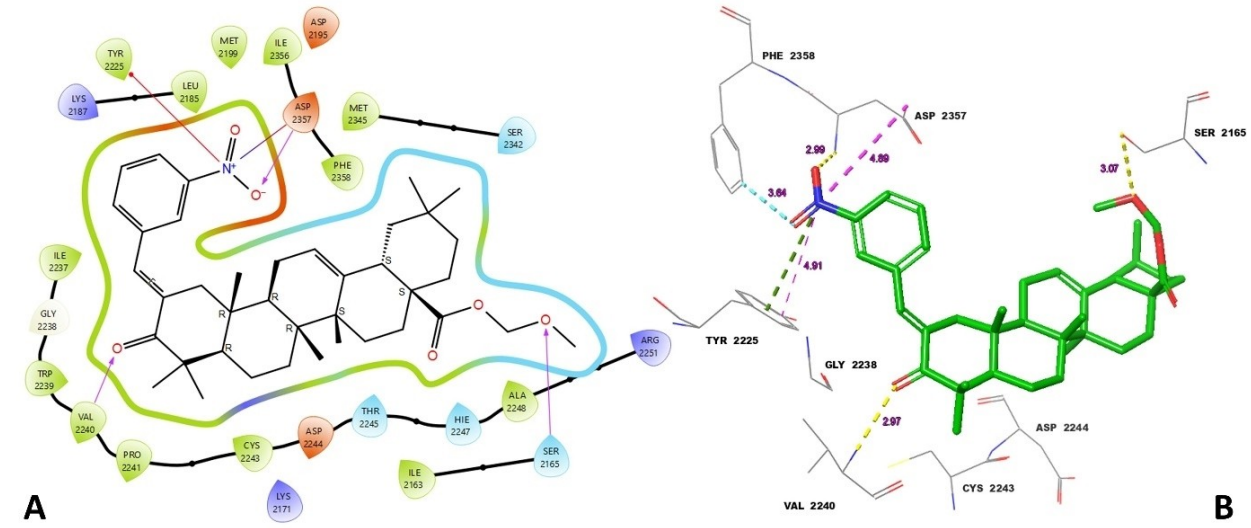

Figure 3. Molecular docking 2D (A) and 3D (B) ligan-protein interactions of **4b-mTOR** complex.

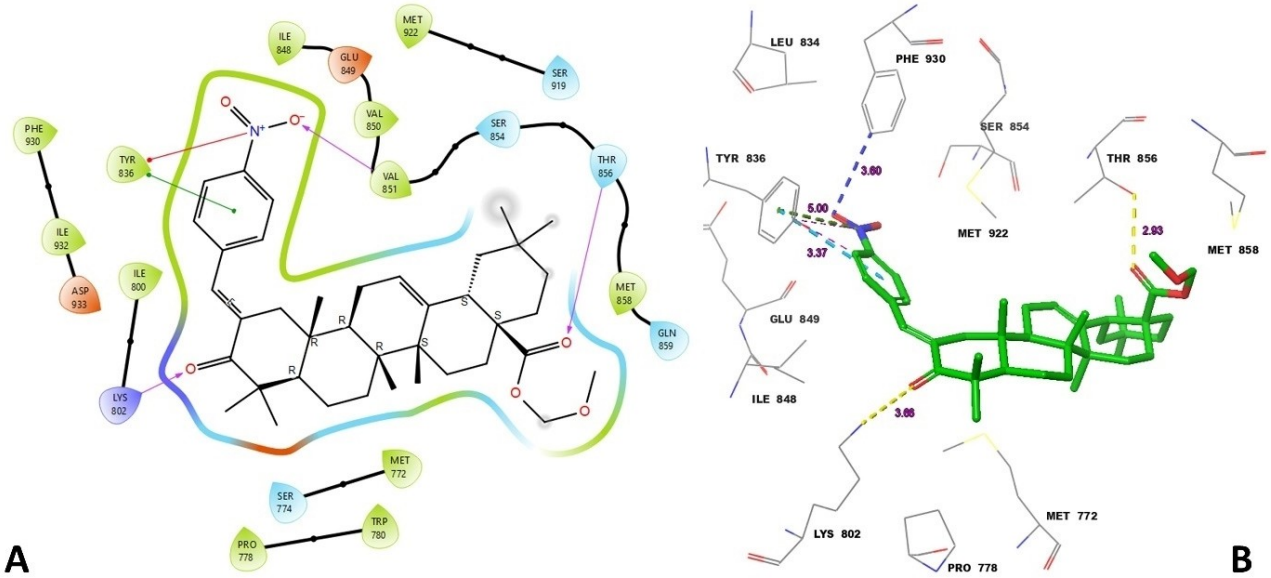

Figure 4. Molecular docking 2D (A) and 3D (B) ligand-protein interactions of **4c-PI3K** complex.

Molecular Dynamics Simulations

To determine the stability of ligand-protein complexes, molecular dynamics (MD) studies were carried out for **4b-PARP1**, **4b-mTOR**, and **4c-PI3K** ligand-protein complexes. In addition, the RMSD (root mean square deviation) values of ligand atoms and proteins were calculated.

The MD simulation analysis of **4b-PARP1**, **4b-mTOR**, and **4c-PI3K** complexes are given in Figures 5, 6, and 7, respectively. In Figures 5, 6, and 7; (A) the 2D key interactions of MD simulation of related complex. (B) RMSD values of ligand atoms and protein Cα atoms of related complex. The left y-axis represents the Root Mean Square Deviation (RMSD) of Protein Cα (blue), while the right y-axis represents the RMSD of the ligand fit on the protein (red). The pink line represents the RMSD of the ligand, indicating its deviation from its reference conformation. (C) MD interaction fraction histograms of the related complexes. Figure 5 presents the analysis of the MD simulation for the **4b-PARP1** complex. According to Figure 5A, hydrogen bond interactions between the oxygens of the nitro group and Ser-904 (21% and 47% of simulation times) and Gly-863 (26% and 47% of simulation times) were observed. In addition, the nitrogen atom of the nitro group interacted with His-862 via a cation-π interaction (16% of simulation time). The ketone's carbonyl group oxygen formed three water-bridged hydrogen bond interactions with Glu-988 (22% of simulation time), Lys-903 (57% of simulation time), and Tyr-907 (19% of simulation time). Furthermore, the oxygen atom of the MOM group formed hydrogen bonds with Arg-865 in 24% and 33% of simulation times. Figure 5B displays the RMSD plots for the

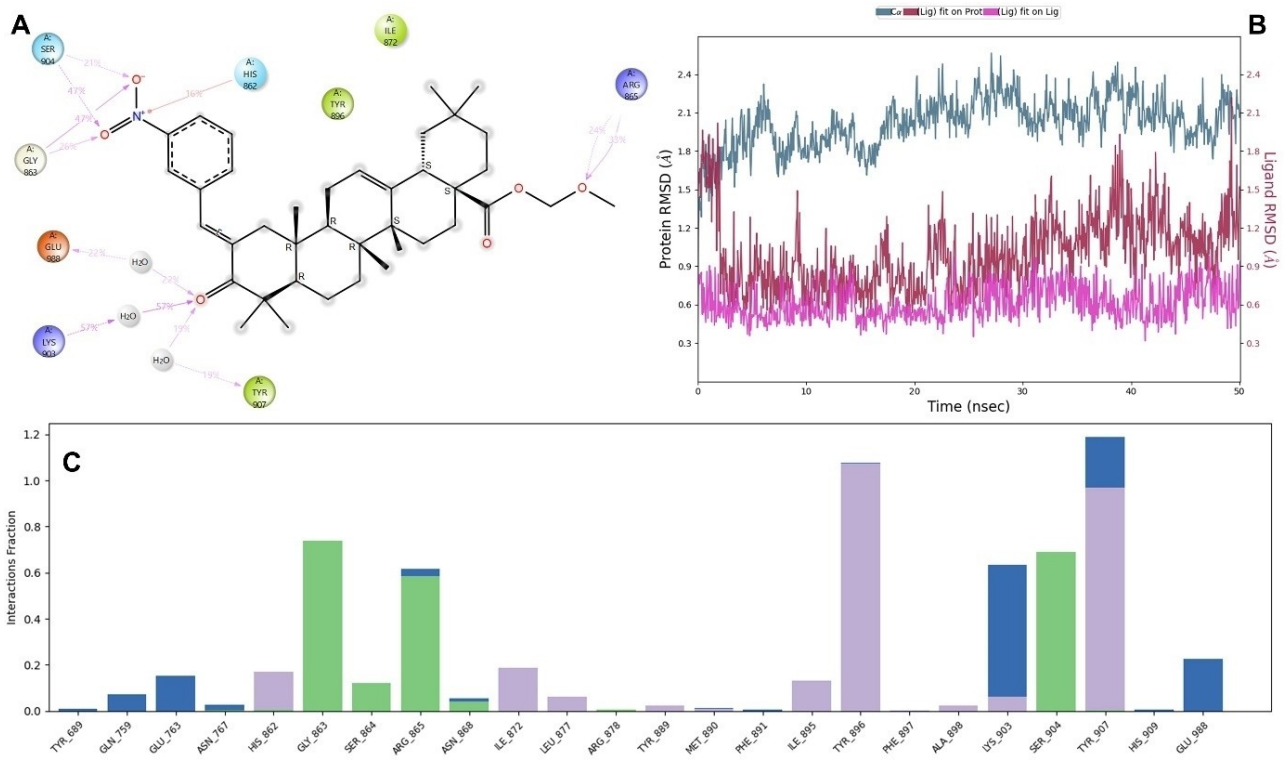

Figure 5. MD simulation analysis of **4b-PARP1** complex (PDB ID: 5WS1).

ligand and protein. It was found that the average RMSD value for protein Cα was 1.8 Å (pale blue), whereas the average RMSD value for ligand fit on protein was 1.1 Å (red). In addition, the RMSD value for 'Lig fit Lig' was estimated to be 0.7 Å (pink). Figure 5C depicts the interaction fractions of the ligand with key residues of the protein over a 50 ns simulation time. Hydrogen bonds (green columns), hydrophobic interactions (purple columns), and water-bridged hydrogen bonds (blue columns) were used to label the interactions. Based on Figure 5C, the most common interactions were observed with Tyr-907 (relative abundance more than 100%), Ser-904 (relative abundance more than 70%), Lys-903 (relative abundance more than 60%), Tyr-896 (relative abundance more than 100%), Arg-865 (relative abundance more than 60%), and Gly-863 (relative abundance more than 70%). A relative abundance greater than 100% shows that certain protein residues belonging to the same subtype have the ability to interact with the ligand multiple times.

The MD simulation analysis of **4b-mTOR** complex was shown in Figure 6.

According to Figure 6A, the oxygens of nitro group on the phenyl ring formed two hydrogen bond interactions with Gly-2238 (13% and 19% of simulation times). The nitrogen atom of the nitro group on the phenyl ring also showed a cation-π interaction with Asp-2195 (13% of simulation time). The phenyl ring formed two π-π stacking interactions with Tyr-2225 (20% of simulation time) and Phe-2358 (5% of simulation time). The carbonyl group oxygen of the ketone interacted with Val-2240 via a hydrogen bond interaction in 96% of the simulation time. The carbonyl group oxygen of the ester moiety formed a water-bridged hydrogen bond interaction with Ser-2165 (6% of simulation time). In addition, the oxygen atom of MOM group interacted with Ser-2165 (5% of simulation time) and Lys-2187 (5% of simulation time) via two water-bridged hydrogen bond interactions. Based on Figure 6B, the average RMSD values were 4.8 Å and 5.5 Å for protein Cα (pale blue) and ligand fit on protein (red), respectively. Additionally, the RMSD value of 'Lig fit Lig' (pink) was found to be 0.8 Å. In Figure 6C, the most abundant interactions were as follows: Ile-2356 (almost 40% relative abundance), Val-2240 (more than 100% relative abundance), Trp-2239 (more than 70% relative abundance), Gly-2238 (more than 30% relative abundance), Ile-2237 (almost 40% relative abundance), and Tyr-2225 (more than 50% relative abundance).

The MD simulation analysis of the **4c-PI3K** complex is given in Figure 7. According to Figure 7A, the oxygen of the nitro group formed a hydrogen bond interaction with Val-851 (85% of the simulation time). The nitrogen atom of the nitro group interacted with Tyr-836 via a cation-π interaction in 87% of the simulation time. The Tyr-836 also formed a π-π stacking interaction with the phenyl ring (93% of simulation time). The carbonyl group oxygen of the ketone moiety formed two water-bridged hydrogen bond interactions with Asp-933 (68% of simulation time) and Lys-802 (67% of simulation time). The carbonyl group oxygen of the ester moiety interacted with Thr-856 via hydrogen bond interaction (20% of simulation time). In addition, the carbonyl group oxygen of the ester moiety formed a water-bridged hydrogen bond interaction with Thr-856 (28%

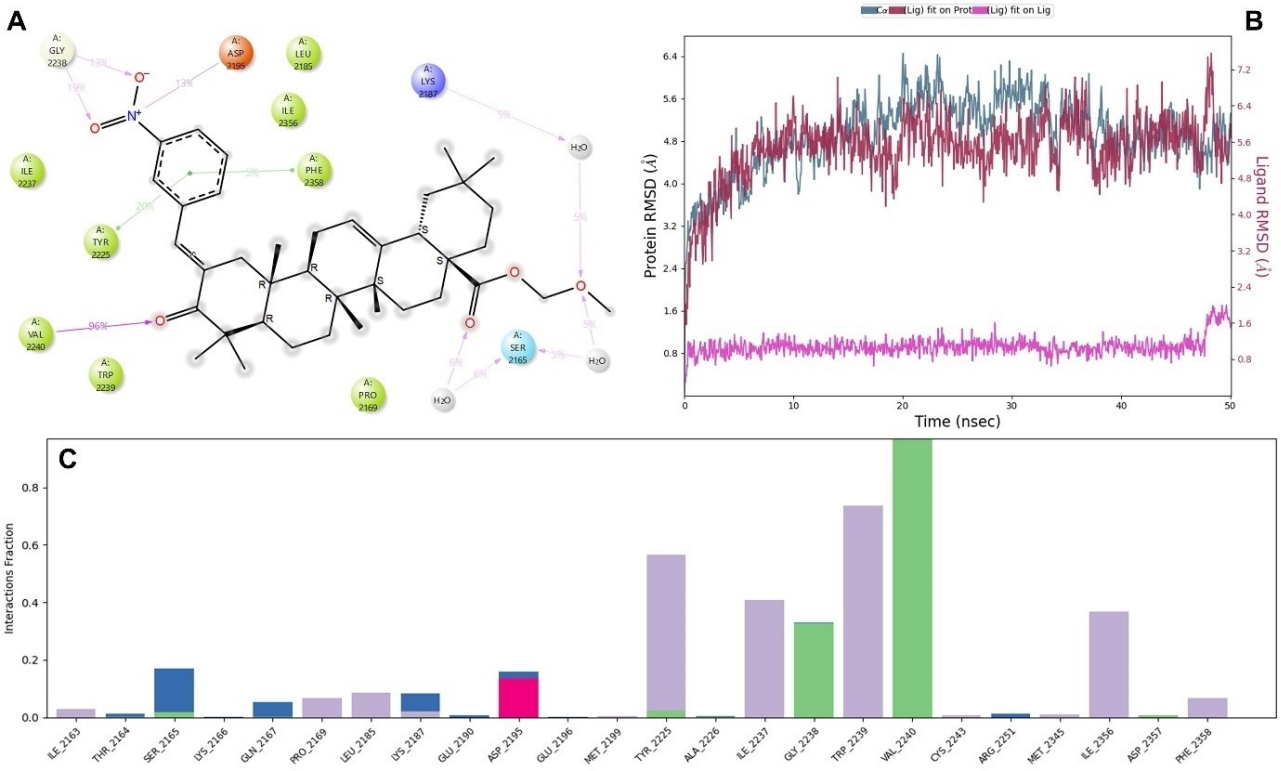

Figure 6. MD simulation analysis of **4b-mTOR** complex (PDB ID: 4JT5).

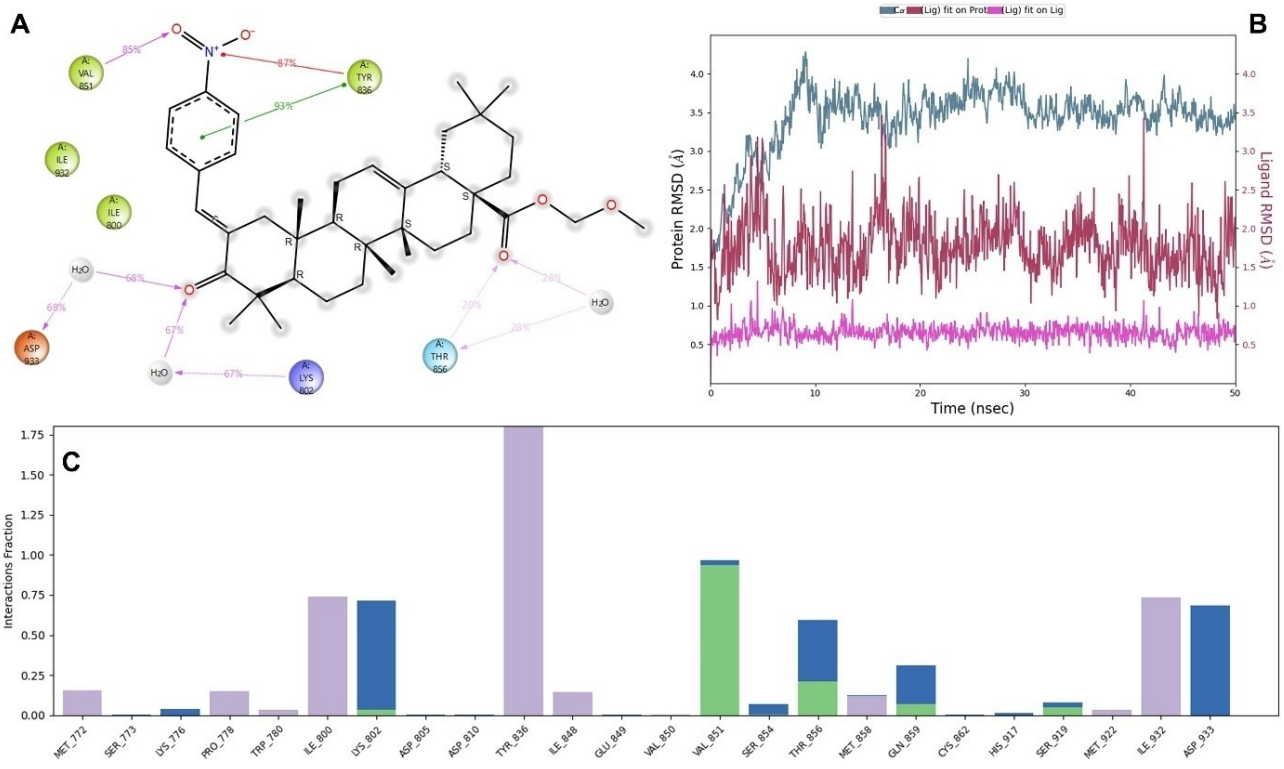

Figure 7. MD simulation analysis of **4c-PI3K** complex (PDB ID: 4L23).

of the simulation time). In Figure 7B, the average RMSD value for protein Cα was 3.5 Å (pale blue), whereas the average RMSD value for ligand fit on protein was 1.8 Å (red). In addition, the RMSD value for 'Lig fit Lig' was found to be 0.5 Å (pink). In

Figure 7C, the most abundant interactions were observed with Asp-933 (almost 70% relative abundance), Ile-932 (more than 70% relative abundance), Gln-859 (more than 50% relative abundance), Thr-856 (more than 70% relative abundance), Val-851 (almost 100% relative abundance), Tyr-836 (more than 100% relative abundance), Lys-802 (more than 70% relative abundance), and Ile-800 (more than 70% relative abundance). According to the RMSD values obtained from MD simulations of ligand-protein complexes, the most stable complex was determined to be **4b-PARP1.**

In addition, the molecular dynamics simulation analysis of **4c-PARP1**, **4e-PARP1**, **4c-mTOR**, **4e-mTOR**, **4b-PI3K**, and **4e-PI3K** complexes are also given in the supplementary material.

In silico ADME studies

ADME (absorption, distribution, metabolism, and elimination) calculations are essential for improving the pharmacokinetic characteristics of novel drugs.[30] The pharmacokinetic properties of the most active compounds (**4b**, **4c**, and **4e**) were determined using the QikProp module of Schrödinger Maestro 13.5. The ADME molecular descriptors, including molecular weight, number of hydrogen bond donors and acceptors, octanol/water partition coefficient, aqueous solubility, Caco-2 cell permeability, brain/blood partition coefficient, MDCK cell permeability, and human oral absorption values, are presented in Table 3.

There are certain rules, such as Lipinski's 5 Rule (RO5) and Jorgensen's 3 Rule (RO3), that have been defined as the criteria for selecting a molecule as a potential drug candidate.[31] According to Lipinski's 5 rule, an orally active drug should not violate more than one of the following criteria: no more than 5 H-bond donors, no more than 10 H-bond acceptors, a molecule with a molecular weight less than 500 Da, and an octanol-water partition coefficient less than 5.[32] Similarly, the number of violations of Jorgensen's 3 Rule was taken into consideration, and the three rules are as follows: aqueous solubility more than−5.7, caco-2 cell permeability more than22, and primary metabolitesless than7. Oral bioavailability of drug candidates will have fewer (and preferably no) violations of these principles.[33]

According to Table 3, the molecular weight values of the compounds ranged from 616.879 to 722.850. The MW values of the most active compounds exceeded 500 and thus did not meet Lipinski's rule of five. The QPlogPo/w values of the title compounds fell within the range of 7.313 to 10.325. However, all of the title compounds had a QPlogPo/w value greater than 5, indicating that they did not match Lipinski's rule of five. According to Lipinski's rule of five, the number of hydrogen bond donors (donorHB) should be less than or equal to 5, and the number of hydrogen bond acceptors (accptHB) should be less than or equal to 10. The QPlogS values of the title compounds ranged from −9.093 to −12.380, which was less than −5.7 and did not comply with Jorgensen's rule of three. All of the title compounds and the reference drug had QPPCaco values greater than 22 and obeyed Jorgensen's rule of three. In summary, the ADME calculations suggested that the most active compounds matched the drug-likeness requirements validated by both Lipinski's and Jorgensen's rules. Therefore, the synthesized title compounds can be considered promising candidates for the development of more potent prostate cancer inhibitors.

Molecular docking validation studies

The co-crystallized ligands of 5WS1 (7U9), 4JT5 (P2X), and 4L23 (X6K) were re-docked at their actual crystal positions without changing their states or producing any conformers, thereby

Table 3. Predicted ADME parameters.

Compounds	4b	4c	4e	Dox*	Rec. Values
Mol. Weight	631.85	631.85	654.85	543.52	130–725
Donor H Bond	0.000	0.000	0.000	5	0–6
Accept H Bond	6.700	6.700	5.700	14	2-20
QPlogPo/w	7.510	7.407	9.285	−0.52	−2–6.5
QPlogS	−9.427	−9.093	−10.912	−2.28	−6.5–0.5
QPlogBB	−1.418	−1.341	−0.044	−2.82	−3–1.2
QPPCaco	352	382	2954	3	<25 poor, >500 great
QPPMDCK	160	174	7056	1	<25 poor, >500 great
%HOA	90	90	100	0	>80 high, <25 poor
Rule of Five	2	2	2	3	maximum is 4
Rule of Three	1	1	1	2	maximum is 3

* Dox = Doxorubicin; QPlogPo/w: predicted octanol/water partition coefficient; QPlogS: prediction of aqueous solubility in mol/L; QPPCaco: predicted Caco-2 cell permeability in nm/sec; QPlogBB: predicted brain/blood partition coefficient; QPPMDCK: predicted apparent MDCK cell permeability in nm/sec; %Human-Oral Absorption: predicted human oral absorption on 0 to 100% scale; Rule of 5: Number of violations of Lipinski's rule of five. The rules are: MW < 500, QPlogPo/w < 5, donorHB ≤ 5, accptHB ≤ 10; Rule of 3: Number of violations of Jorgensen's rule of three. The three rules are: QPlogS > −5.7, QPPCaco > 22 nm/s, # Primary Metabolites < 7.

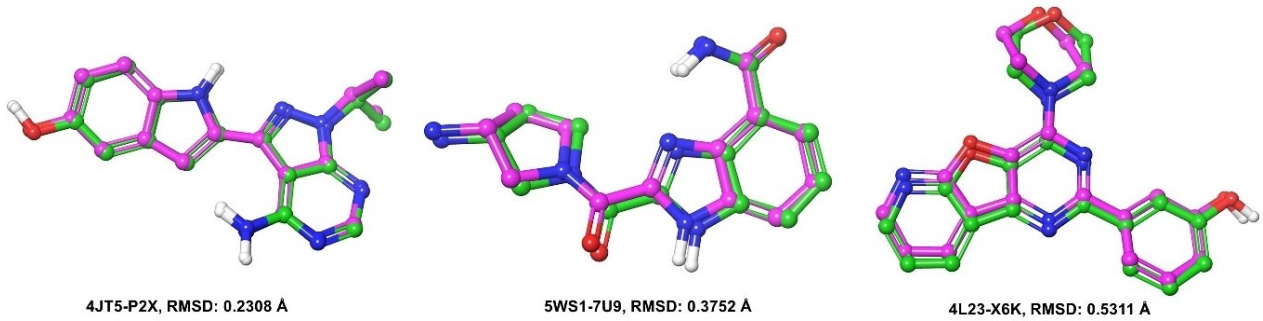

Figure 8. Docking validation images of 4JT5, 5WSQ and 4L2.

validating the molecular docking methods and protocols.[26] The original crystallographic conformation was superimposed with the co-crystallized ligand's docked pose, and the RMSD was found to be 0.3752 Å for 5WS1, 0.2308 Å for 4JT5, and 0.5311 Å for 4L23. Docking validation images are given in Figure 8.

Conclusions

Prostate cancer is the most frequently seen cancer in men and has been increasing worldwide. It is expected that it will continue growing in many countries. Therefore, the development of new agents for its treatment is urgently required. In this study, a series of α,β-unsaturated ketones based on oleanolic acid (**4a–i**) were synthesized, and evaluated for their biological activity. The synthesized compounds were characterized using ^{1}H and ^{13}C-NMR, FTIR, and HRMS techniques. The human prostate cancer (PC3) cell lines was employed to test the anticancer activity of new compounds *in vitro* using the MTT assay, while the human umbilical vein endothelial cell (HUVEC) was used as a healthy control. According to the findings of the *in vitro* biological activity studies, the IC_{50} values for the title compounds (**4a–i**) and doxorubicin (DOX) as a reference drug against healthy cells ranged from 9.06 to 84.58 μM. In comparison to DOX, title compounds showed significantly lower toxicity toward healthy cells. The title compounds and DOX had IC_{50} values varying from 5.33 to 17.62 M when evaluated against PC3 cancer cells. The IC_{50} values of the title compounds were higher than the values of the reference drug DOX, but the selectivity index of DOX was very low (1.7). The compounds with the highest selectivity index on PC3 cell lines were **4b** (7.48), **4c** (9.54), and **4e** (7.97). The SAR study demonstrated that the position and nature of phenyl ring substituents can influence biological activity. Compounds having a CF_3 and a NO_2 at *meta*- or *para*- positions on the phenyl ring exhibited higher potency. In order to explore the drug-likeness characteristics, *in silico* ADME calculations were performed for the most potent commands (**4b**, **4c**, and **4e**) and DOX. The results of the ADME analysis showed that the drug-likeness parameters were within the defined ranges according to Lipinski's and Jorgensen's rules. For the most potent compounds **4b**, **4c**, and **4e**, a molecular docking analysis by means of an induced fit docking (IFD) protocol was performed against three protein targets, namely PARP1 (PDB ID: 5WS1), PI3K (PDB ID: 4L23), and mTOR (PDB ID: 4JT5). According to the IFD scores, compound **4b** had the highest calculated affinity for the protein target PARP1 (IFD score: −10.505 kcal/mol), while compound **4c** had higher affinities for the protein targets mTOR and PI3K (IFD scores: −10.291 and −10.897 kcal/mol, respectively). In addition, the docking analysis showed that the most potent compounds (**4b**, **4c**, and **4e**) fit very well into the active site of the protein targets, which makes stable complexes. The MM-GBSA calculations showed that the most active compounds **4b**, **4c**, and **4e** had high binding affinities and formed stable ligand-receptor complexes with the protein targets. Finally, a 50 ns molecular dynamics (MD) simulation was performed to study the behavior of protein target complexes under in silico physiological conditions. The results revealed high stability in the binding pocket of protein targets for the most active compounds. These findings suggest that compounds **4b**, **4c**, and **4e** are promising potential candidates for the development of prostate cancer inhibitors.

Experimental Section

Materials

All chemicals and solvents utilized in this study were of analytical grade, were used without additional purification, and were purchased from Sigma-Aldrich, Merck, 1pluschem, and Tekkim. Thin-layer chromatography (TLC) using TLC plates with aluminum backed silica gel 60 F_{254} was used to monitor the progress of the reactions. The spots were detected using UV light, a 10% cerium (IV) sulfate solution in sulfuric acid, and heating on a burner at 100 °C. ^{1}H-NMR, ^{13}C APT NMR, COSY, HSQC, HMBC, and ^{19}F NMR spectra were recorded on a Bruker Avance NEO Spectrometer operating at 500 MHz for ^{1}H-NMR, 125 MHz for ^{13}C-NMR, and 471 MHz for ^{19}F NMR in $CDCl_3$ with tetramethylsilane (TMS) as an internal standard. The values of coupling constants (*J*) and chemical shifts (δ) were mentioned in and ppm, respectively. The FT-IR spectra were obtained on the Bruker ALPHA II FTIR Spectrometer. HRMS spectra were recorded using the ESI technique by the Thermo Fischer Scientific Q Exactive™ Hybrid Quadrupole-Orbitrap™ Mass Spectrometer. All melting points of the synthesized compounds were determined using a Stuart SMP30 melting point instrument. Column chromatography separations were performed using silica gel 60 (0.063–0.200 mm, 70–230 mesh; ASTM).

Synthesis of methoxymethyl 3β-hydroxyolean-12-en-28-oate (2)

In a round-bottomed flask, a mixture of tetrahydrofuran (THF) and sodium hydride (NaH, 2.1 g, 52 mmol, 2 equiv.) was placed and cooled to 0–5 °C by use of an ice bath. Oleanolic acid (12 g, 26 mmol, 1 equiv.) was added to the flask, and the resulting mixture was stirred for 30 min. After this time, bromomethyl methyl ether (MOMBr, 3.94 g, 2.45 mL, 32 mmol, 1.2 equiv.) was added to the solution, and the mixture was stirred for 6 h under N_2. The reaction's progression was monitored by TLC. After completion of the reaction, the excess NaH was carefully destroyed by the addition of water (5 mL). Finally, the solution was concentrated by a rotary evaporator, and the resulting mixture was washed with water (3×300 mL) and extracted with chloroform (3×300 mL). The organic layers were combined and dried over anhydrous Na_2SO_4, filtered, and concentrated under reduced pressure. The crude mixture was purified by column chromatography on silica gel eluted with hexane-ethyl acetate (9:1 v/v) to afford target compound **2**: White solid, 13.0 g, 99% yield. **m.p.**: 260–261 °C;[14f] **^{1}H-NMR (500 MHz, $CDCl_3$) δ** 5.32 (d, *J* = 3.8, 1H), 5.25 (d, *J* = 6.0, 1H), 5.18 (d, *J* = 5.9, 1H), 3.47 (s, 3H), 3.22 (dd, *J* = 11.5, 4.5, 1H), 2.90 (dd, *J* = 14.0, 4.6, 1H), 2.00 (td, *J* = 14.7, 4.1, 1H), 1.89 (dt, *J* = 11.4, 3.4, 2H), 1.16 (s, 3H), 1.00 (s, 3H), 0.95 (s, 3H), 0.92 (d, *J* = 2.3, 5H), 0.79 (s, 3H), 0.77 (s, 3H); **^{13}C-NMR (125 MHz, $CDCl_3$) δ** 177.24, 143.63, 122.55, 90.45, 79.00, 57.60, 55.22, 47.61, 46.97, 45.85, 41.74, 41.21, 39.35, 38.76, 38.46, 37.03, 33.86, 33.10, 32.77, 32.39, 30.71, 28.12, 27.62, 27.19, 25.86, 23.62, 23.43, 22.95, 18.34, 16.99, 15.60, 15.33.

Synthesis of methoxymethyl 3-oxo-olean-12-en-28-oate (3)

In a round-bottomed flask, a mixture of pyridinium chlorochromate (PCC, 12 g, 52 mmol, 2 equiv.) and dichloromethane (DCM, 200 mL) was added to a solution of compound **2** (13 g, 26 mmol, 1 equiv.) in DCM (250 mL). The reaction mixture was stirred on a magnetic stirrer at room temperature overnight. The TLC experiments were performed to monitor the progress of the reaction. After the reaction was complete, the mixture was concentrated using a rotary evaporator under reduced pressure. The crude mixture was purified by silica gel column chromatography using hexane-ethyl acetate (9:1 v/v) as an eluent to obtain target compound **3**: White solid, 11.0 g, 85% yield. **m.p.**: 118–120 °C; **^{1}H-NMR (500 MHz, $CDCl_3$) δ** 5.07 (t, *J* = 3.8, 1H), 4.98 (d, *J* = 5.9, 1H), 4.91 (d, *J* = 5.9, 1H), 3.20 (s, 3H), 2.64 (dd, *J* = 13.9, 4.6, 1H), 2.28 (ddd, *J* = 15.9, 11.1, 7.3, 1H), 2.10 (ddd, *J* = 15.9, 6.8, 3.6, 1H), 1.79–0.60 (m, peak group belongs to aliphatic region, 20H), 0.89 (s, 3H), 0.82 (s, 3H), 0.78 (s, 6H), 0.68 (s, 3H), 0.65 (s, 3H), 0.55 (s, 3H); **^{13}C-NMR (125 MHz, $CDCl_3$) δ** 217.57, 177.11, 143.67, 122.30, 90.40, 57.56, 55.31, 47.41, 46.95, 46.85, 45.78, 41.84, 41.28, 39.32, 39.13, 36.73, 34.13, 33.83, 33.07, 32.31, 32.28, 30.68, 27.60, 26.44, 25.72, 23.57, 23.50, 22.92, 21.47, 19.58, 16.90, 15.01.

General synthesis of desired compounds 4 a–i

General method: In a 250 mL round-bottomed flask, KOH (0.5 g, 9 mmol, 4.5 equiv.) was added to EtOH (30 mL) under stirring at room temperature until complete dissolution. After the synthesized compound **3** (1 g, 2 mmol, 1 equiv.) in THF (30 mL) was added to the flask, an appropriate amount of the corresponding aromatic aldehyde (3 mmol, 1.5 equiv.) was added to the reaction system. The mixture was stirred for 12 h at room temperature. After the reaction was completed (controlled by TLC), the mixture was concentrated under reduced pressure using a rotary evaporator. The crude mixture was purified by column chromatography over silica gel eluted with hexane-ethyl acetate (9:1 v/v) to get the title compounds **4 a–i**.

Methoxymethyl 3-oxo-2-(2-nitro-benzylidene)-olean-12-ene-28-oate (***4 a***)*:* Starting with 2-nitrobenzaldehyde (330 mg); White solid, 0.9 g, 71% yield. **m.p.**: 177–178 °C; **^{1}H-NMR (500 MHz, $CDCl_3$) δ** 8.12 (d, *J* = 8.2, 1H), 7.65 (d, *J* = 5.9, 2H), 7.51 (t, *J* = 7.9, 1H), 7.30 (d, *J* = 8.2, 1H), 5.27 (s, 1H), 5.23 (d, *J* = 5.8, 1H), 5.17 (d, *J* = 5.9, 1H), 3.45 (s, 3H), 2.88 (dd, *J* = 13.9, 4.6, 1H), 2.62 (d, *J* = 15.6, 1H), 1.98 (d, *J* = 14.8, 2H), 1.90–0.80 (m, peak group belongs to aliphatic region, 17H),1.21 (s, 3H), 1.17 (s, 3H), 1.16 (s, 3H), 0.92 (s, 3H), 0.89 (s, 6H), 0.80 (s, 3H); **^{13}C-NMR (125 MHz, $CDCl_3$) δ** 207.26, 177.12, 148.16, 143.84, 135.78, 133.99, 133.13, 132.21, 130.98, 128.86, 124.91, 122.04, 90.45, 57.59, 53.55, 47.02, 45.88, 45.83, 45.27, 42.89, 42.02, 41.41, 39.27, 36.73, 33.82, 33.06, 32.27, 32.05, 30.68, 28.93, 27.57, 25.61, 23.58, 23.46, 22.96, 22.81, 20.14, 16.68, 15.16; **FT-IR** (cm^{-1}) ν_{max}: 3050, 2979, 2916, 1731, 1716, 1672, 1604, 1586, 1518, 1440, 1383, 1366, 1301, 1246, 1197, 1059, 1015, 960, 869, 793, 750; **HR-ESI-MS** *m/z*: Chemical Formula: $C_{39}H_{53}NO_6$, Exact Mass: *m/z* 631.38729, Calculated *m/z* $[M+Na]^+$: 654.37706, Found *m/z* $[M+Na]^+$: 654.37586.

Methoxymethyl 3-oxo-2-(3-nitro-benzylidene)-olean-12-ene-28-oate (***4 b***)*:* Starting with 3-nitrobenzaldehyde (330 mg); White solid, 1.1 g, 86% yield. **m.p.**: 157–159 °C; **^{1}H-NMR (500 MHz, $CDCl_3$) δ** 8.27 (d, *J* = 2.0, 1H), 8.19 (dd, *J* = 8.2, 2.2, 1H), 7.71 (d, *J* = 7.7, 1H), 7.59 (t, *J* = 8.0, 1H), 7.53 (d, *J* = 2.8, 1H), 5.37 (t, *J* = 3.7, 1H), 5.25 (d, *J* = 5.9, 1H), 5.19 (d, *J* = 5.9, 1H), 3.47 (s, 3H), 3.03–2.94 (m, 1H), 2.33 (dd, *J* = 16.3, 3.1, 1H), 2.03 (td, *J* = 14.3, 13.7, 4.0, 1H), 1.97–1.92 (m, 2H), 1.80–0.80 (m, peak group belongs to aliphatic region, 16H), 1.23 (s, 3H), 1.20 (s, 3H), 1.18 (s, 3H), 0.96 (s, 3H), 0.94 (s, 3H), 0.89 (s, 3H), 0.83 (s, 3H); **^{13}C-NMR (125 MHz, $CDCl_3$) δ** 207.41, 177.18, 148.27, 143.67, 137.56, 136.52, 135.91, 134.41, 129.43, 124.44, 122.96, 122.16, 90.44, 57.61, 53.06, 47.03, 45.74, 45.37, 43.78, 42.01, 41.40, 39.27, 36.46, 33.87, 33.07, 32.31, 31.90, 30.72, 29.58, 27.61, 25.58, 23.60, 23.57, 22.98, 22.71, 20.33, 16.62, 15.35; **HSQC Correlations**: 124.35–8.27, 124.35–8.19, 135.94–7.71, 129.46–7.59, 134.46–7.53, 122.27-5.37, 90.30–5.25, 90.18–5.19, 57.61–3.47, 43.85–3.47, 44.21–2.99, 41.37–2.95, 41.39–2.95, 43.78–2.92, 43.98–2.35, 45.39–2.31, 45.48–1.95, 45.91–1.77, 45.91–1.72, 45.94–1.69, 53.10–1.67, 33.86–1.53–1.37, 45.55–1.26, 33.82–1.25, 45.93–1.23, 25.60–1.23, 22.77–1.20, 29.66–1.18, 23.60–0.96, 33.13–0.94, 33.13–0.94, 15.44–0.89, 16.67–0.83; **FT-IR** (cm^{-1}) ν_{max}: 3050, 2947, 2914, 1736, 1678, 1596, 1568, 1530, 1469, 1382, 1320, 1257, 1170, 1026, 998, 988, 875, 734; **HR-ESI-MS** *m/z*: Chemical Formula: $C_{39}H_{53}NO_6$, Exact Mass: *m/z* 631.38729, Calculated *m/z* $[M+H]^+$: 632.39511, Found *m/z* $[M+Na]^+$: 632.39496.

Methoxymethyl 3-oxo-2-(4-nitro-benzylidene)olean-12-ene-28-oate (***4 c***). Starting with 4-nitrobenzaldehyde (0.6 g); White solid, 1.5 g, 79% yield. **m.p.**: 102–104 °C; **^{1}H-NMR (500 MHz, $CDCl_3$) δ** 7.95 (d, *J* = 8.7, 2H), 7.27 (d, *J* = 8.6, 2H), 7.22 (d, *J* = 2.8, 1H), 5.08 (t, *J* = 3.7, 1H), 4.95 (d, *J* = 6.0, 1H), 4.89 (d, *J* = 5.9, 1H), 3.17 (s, 3H), 2.74–2.65 (m, 1H), 2.66–2.61 (m, 1H), 2.04 (dd, *J* = 16.7, 3.2, 1H), 1.80–0.80 (m, peak group belongs to aliphatic region, 18H), 0.93 (s, 3H), 0.90 (s, 3H), 0.87 (s, 3H), 0.65 (s, 3H), 0.63 (s, 3H), 0.58 (s, 3H), 0.54 (s, 3H); **^{13}C-NMR (125 MHz, $CDCl_3$) δ** 207.37, 177.11, 147.09, 143.88, 142.45, 137.30, 134.52, 130.69, 123.62, 122.04, 90.43, 57.59, 53.06, 47.02, 45.83, 45.38, 45.32, 44.08, 42.05, 41.43, 39.27, 36.39, 33.84, 33.08, 32.27, 31.91, 30.71, 29.57, 27.57, 25.61, 23.69, 23.58, 22.97, 22.71, 20.30, 16.61, 15.34; **FT-IR** (cm^{-1}) ν_{max}: 3050, 2944, 2863, 1728, 1679, 1592, 1490, 1460, 1380, 1306, 1281, 1194, 1072, 1014, 997, 813, 751; **HR-ESI-MS** *m/z*: Chemical Formula: $C_{39}H_{53}NO_6$, Exact Mass: *m/z* 631.38729, Calculated *m/z* $[M+Na]^+$: 654.37706, Found *m/z* $[M+Na]^+$: 654.37659.

Methoxymethyl 3-oxo-2-(3-trifluoromethy-benzylidene)-olean-12-ene-28-oate (***4 d***). Starting with 3-trifluoromethylbenzaldehyde (0.7 mg); White solid, 1.05 g, 77% yield. **m.p.**: 93–95 °C; **^{1}H-NMR (500 MHz, $CDCl_3$) δ** 7.54 (s, 1H), 7.52–7.39 (m, 4H), 5.29–5.24 (m, 1H), 5.14 (d, *J* = 6.0, 1H), 5.07 (d, *J* = 6.0, 1H), 3.35 (s, 3H), 2.93–2.86 (m, 1H), 2.83 (dd, *J* = 14.1, 4.6, 1H), 2.24–2.16 (m, 1H), 1.91 (dt, *J* = 14.6, 7.3, 2H), 1.85 (dd, *J* = 9.1, 3.5, 2H), 1.70–0.70 (m, peak group

belongs to aliphatic region, 14H), 1.12 (s, 3H), 1.08 (s, 3H), 1.06 (s, 3H), 0.84 (s, 3H), 0.82 (s, 3H), 0.78 (s, 3H), 0.73 (s, 3H); **^{13}C-NMR (125 MHz, CDCl$_3$) δ** 207.55, 177.19, 143.72, 136.67, 135.60, 135.47, 132.98, 130.88 (q, *J* = 32.3, *131.26*, *131.01*, *130.75*, *130.49*) 128.90, 126.87 (q, *J* = 3.8, *126.92*, *126.89*, *126.86*, *126.83*), 124.91 (q, *J* = 3.6, *124.95*, *124.93*, *124.90*, *124.87*), 123.95 (q, *J* = 272.5, *127.20*, *125.04*, *122.87*, *120.70*), 122.23, 90.46, 57.61, 53.10, 47.03, 45.79, 45.40, 45.34, 43.72, 42.00, 41.39, 39.28, 36.44, 33.87, 33.08, 32.32, 31.92, 30.73, 29.57, 27.62, 25.62, 23.57, 22.98, 22.73, 20.34, 16.62, 15.29; **FT-IR (cm^{-1}) ν$_{max}$**: 3070, 2945, 2865, 1728, 1679, 1599, 1460, 1383, 1328, 1257, 1204, 1146, 1094, 1019, 952, 799, 698, 571; **HR-ESI-MS** *m/z*: Chemical Formula: $C_{40}H_{53}F_3O_4$, Exact Mass: *m/z* 654.38959, Calculated *m/z* $[M+H]^+$: 655.39742, Found *m/z* $[M+H]^+$: 655.39569.

Methoxymethyl 3-oxo-2-(4-trifluoromethy-benzylidene)-olean-12-ene-28-oate (***4e***). Starting with 4-trifluoromethylbenzaldehyde (0.7 g); White solid, 1.07 g, 81% yield. **m.p.**: 105–107 °C; **^{1}H-NMR (500 MHz, CDCl$_3$) δ** 7.66 (d, *J* = 8.1, 2H), 7.53 (s, 1H), 7.51 (d, *J* = 8.2, 2H), 5.38 (t, *J* = 3.7, 1H), 5.26 (d, *J* = 5.9, 1H), 5.19 (d, *J* = 5.9, 1H), 3.47 (s, 3H), 3.03–2.89 (m, 2H), 2.30 (dd, *J* = 16.3, 3.2, 1H), 2.03 (td, *J* = 14.2, 13.7, 4.0, 1H), 1.96 (dd, *J* = 9.1, 3.6, 2H), 1.80–1.00 (m, peak group belongs to aliphatic region 15H) 1.23 (s, 3H), 1.20 (s, 3H), 1.17 (s, 3H), 0.96 (s, 3H), 0.94 (s, 3H), 0.88 (s, 3H), 0.84 (s, 3H); **^{13}C-NMR (125 MHz, CDCl$_3$) δ** 207.59, 177.16, 143.87, 139.45, 135.85, 135.57, 130.00 (q, *J* = 32.9, *130.39*, *130.13*, *129.87*, *129.61*), 130.26, 124.91 (q, *J* = 272.1, *127.24*, *125.08*, *122.91*, *120.75*), 125.31 (q, *J* = 3.7, *125.35*, *125.32*, *125.29*, *125.26*), 122.16, 90.46, 57.61, 53.09, 47.05, 45.87, 45.35, 45.32, 44.00, 42.07, 41.46, 39.28, 36.35, 33.86, 33.08, 32.30, 31.96, 30.72, 29.63, 27.60, 25.63, 23.70, 23.59, 22.99, 22.71, 20.33, 16.63, 15.29; **FT-IR (cm^{-1}) ν$_{max}$**: 3050, 2945, 2907, 2864, 1728, 1679, 1601, 1460, 1383, 1321, 1228, 1165, 1068, 952, 855, 781, 735, 648; **HR-ESI-MS** *m/z*: Chemical Formula: $C_{40}H_{53}F_3O_4$, Exact Mass: *m/z* 654.38959, Calculated *m/z* $[M+H]^+$: 655.39742, Found *m/z* $[M+H]^+$: 655.39665, Calculated *m/z* $[M+Na]^+$: 677.37936, Found *m/z* $[M+Na]^+$: 677.37860.

Methoxymethyl 3-oxo-2-(3,5-bis(trifluoromethyl)-benzylidene)-olean-12-ene-28-oate (***4f***). Starting with 3,5-bistrifluoromethylbenzaldehyde (0.55 g); White solid, 1.27 g, 87% yield. **m.p.**: 199–200 °C; **^{1}H-NMR (500 MHz, CDCl$_3$) δ** 7.74 (s, 1H), 7.73 (s, 2H), 7.43 (s, 1H), 5.26 (t, *J* = 3.7, 1H), 5.15 (d, *J* = 5.9, 1H), 5.09 (d, *J* = 5.9, 1H), 3.37 (s, 3H), 2.90–2.81 (m, 2H), 2.18 (d, *J* = 15.4, 1H), 2.00–0.90 (m, peak group belongs to aliphatic region 18H) 1.13 (s, 3H), 1.13 (s, 3H), 1.09 (s, 3H), 0.86 (s, 3H), 0.84 (s, 3H), 0.81 (s, 3H), 0.73 (s, 3H); **^{13}C-NMR (125 MHz, CDCl$_3$) δ** 206.99, 177.12, 143.56, 143.40, 137.98, 137.26, 133.66, 131.79 (q, *J* = 33.4, *132.19*, *131.92*, *131.66*, *131.39*), 129.60 (q, *J* = 4 Hz, *129.65*, *129.62*, *129.59*, *129.56*), 123.16 (q, *J* = 272.8, *126.42*, *124.25*, *122.08*, *119.91*), 122.11, 121.75–121.58 (m), 90.42, 57.51, 53.15, 46.95, 45.67, 45.47, 45.44, 43.28, 41.90, 41.29, 39.27, 36.63, 33.86, 33.01, 32.31, 31.82, 30.68, 29.39, 29.34, 28.12, 27.61, 25.57, 23.49, 23.38, 22.93, 22.74, 20.28, 16.57, 15.28; **HSQC Correlations**: 121.64–7.82, 129.61–7.80, 133.70–7.51, 120.64–5.34, 122.17–5.34, 90.46–5.23, 90.42–5.17, 57.52–3.44, 25.59–1.21, 22.75–1.17, 29.35–1.17, 23.53–0.94, 33.03–0.92, 15.31–0.89, 16.59–0.81; **^{19}F NMR (471 MHz, CDCl$_3$)** δ −62.97; **FT-IR (cm^{-1}) ν$_{max}$**: 3050, 2992, 2945, 2838, 1722, 1706, 1680, 1601, 1461, 1453, 1364, 1349, 1246, 1180, 1169, 1058, 1000, 929, 845, 806, 752, 650 ; **HR-ESI-MS** *m/z*: Chemical Formula: $C_{41}H_{52}F_6O_4$, Exact Mass: *m/z* 654.38959, Calculated *m/z* $[M+H]^+$: 655.39742, Found *m/z* $[M+H]^+$: 722.37698, Calculated *m/z* $[M+H]^+$: 723.38480, Found *m/z* $[M+Na]^+$: 723.38501.

Methoxymethyl 3-oxo-2-(4-cyano-benzylidene)-olean-12-ene-28-oate (***4g***). Starting with 4-cyanobenzaldehyde (0.3 g); White solid, 0.9 g, 73% yield. **m.p.**: 107–109 °C; **^{1}H-NMR (500 MHz, CDCl$_3$) δ** 7.60 (d, *J* = 8.3, 2H), 7.41 (d, *J* = 8.4, 2H), 7.40 (s, 1H), 5.30 (t, *J* = 3.8, 1H), 5.17 (d, *J* = 6.0, 1H), 5.10 (d, *J* = 5.9, 1H), 3.38 (s, 3H), 2.86 (dd, *J* = 16.4, 1.7, 2H), 2.21 (dd, *J* = 16.5, 3.2, 1H), 1.94 (td, *J* = 14.3, 13.7, 3.9, 1H), 1.90–1.84 (m, 2H), 1.73–0.90 (m, peak group belongs to aliphatic region 15H),1.14 (s, 3H), 1.11 (s, 3H), 1.08 (s, 3H), 0.88 (s, 3H), 0.85 (s, 3H), 0.79 (s, 3H), 0.75 (s, 3H); **^{13}C-NMR (125 MHz, CDCl$_3$) δ** 207.47, 177.15, 143.96, 140.49, 136.76, 134.98, 132.13, 130.53, 127.83, 122.06, 118.67, 112.29, 90.47, 65.06, 62.63, 57.62, 53.07, 48.04, 47.05, 45.89, 45.36, 44.09, 42.08, 41.45, 39.30, 38.80, 36.38, 33.85, 32.29, 31.93, 30.73, 25.63, 23.71, 23.59, 22.70, 20.32, 16.83, 15.34; **FT-IR (cm^{-1}) ν$_{max}$**: 3033, 2944, 2846, 2226, 1727, 1678, 1600, 1501, 1459, 1383, 1329, 1249, 1212, 1145, 1092, 1016, 927, 804, 752, 660 ; **HR-ESI-MS** *m/z*: Chemical Formula: $C_{40}H_{53}NO_4$, Exact Mass: *m/z* 611.39746, Calculated *m/z* $[M+H]^+$: 612.40528, Found *m/z* $[M+H]^+$: 612.4016.

Methoxymethyl 3-oxo-2-(2-methoxy-benzylidene)-olean-12-ene-28-oate (***4h***). Starting with 2-methoxybenzaldehyde (0.3 g); White solid, 0.95 g, 77% yield. **m.p.**: 85–87 °C; **^{1}H-NMR (500 MHz, CDCl$_3$) δ** 7.74 (d, *J* = 2.7, 1H), 7.29–7.17 (m, 2H), 6.88 (td, *J* = 7.5, 1.1, 1H), 6.83 (dd, *J* = 8.4, 1.1, 1H), 5.27 (t, *J* = 3.7, 1H), 5.16 (d, *J* = 5.9, 1H), 5.10 (d, *J* = 6.0, 1H), 3.76 (s, 3H), 3.38 (s, 3H), 2.88 (d, *J* = 16.4, 2H), 2.84 (dd, *J* = 9.7, 4.6, 1H), 2.12 (dd, *J* = 15.5, 2.8, 1H), 1.93 (td, *J* = 14.1, 13.5, 3.9, 1H), 1.85 (dd, *J* = 8.9, 3.7, 2H), 1.72–0.9 (m, peak group belongs to aliphatic region 15H), 1.13 (s, 3H), 1.09 (s, 6H), 0.86 (s, 3H), 0.84 (s, 3H), 0.79 (s, 3H), 0.74 (s, 3H); **^{13}C-NMR (125 MHz, CDCl$_3$) δ** 207.52, 177.20, 158.47, 143.73, 133.32, 133.25, 129.97, 129.93, 124.95, 122.41, 119.90, 110.68, 90.47, 57.61, 55.50, 53.29, 47.07, 45.86, 45.37, 45.30, 43.76, 42.06, 41.45, 39.30, 36.44, 33.87, 33.09, 32.33, 32.07, 30.72, 29.57, 27.62, 25.66, 23.65, 23.60, 23.00, 22.87, 20.32, 16.70, 15.18; **FT-IR (cm^{-1}) ν$_{max}$**: 3056, 2943, 2905, 2864, 1728, 1674, 1595, 1485, 1460, 1381, 1300, 1244, 1215, 1145, 1091, 1072, 1050, 928, 804, 750, 649; **HR-ESI-MS** *m/z*: Chemical Formula: $C_{40}H_{56}O_5$, Exact Mass: *m/z* 616.41277, Calculated *m/z* $[M+H]^+$: 617.42060, Found *m/z* $[M+H]^+$: 617.42010.

Methoxymethyl 3-oxo-2-(4-methoxy-benzylidene)-olean-12-ene-28-oate (***4i***). Starting with 4-methoxybenzaldehyde (0.3 g); White solid, 0.99 g, 78% yield. **m.p.**: 109–111 °C; **^{1}H-NMR (500 MHz, CDCl$_3$) δ** 7.42 (s, 1H), 7.32 (d, *J* = 8.9, 2H), 6.84 (d, *J* = 8.8, 2H), 5.31 (t, *J* = 3.6, 1H), 5.16 (d, *J* = 6.0, 1H), 5.09 (d, *J* = 6.0, 1H), 3.74 (s, 3H), 3.37 (s, 3H), 2.92 (d, *J* = 16.2, 1H), 2.85 (dd, *J* = 13.9, 4.5, 1H), 2.20 (d, *J* = 15.1, 1H), 2.00–0.9 (m, peak group belongs to aliphatic region 18H), 1.14 (s, 3H), 1.09 (s, 3H), 1.05 (s, 3H), 0.87 (s, 3H), 0.84 (s, 3H), 0.78 (s, 3H), 0.74 (s, 3H); **^{13}C-NMR (125 MHz, CDCl$_3$) δ** 207.75, 177.17, 159.85, 143.82, 137.39, 132.26, 131.51, 128.60, 122.36, 113.94, 90.45, 57.61, 55.30, 52.87, 47.06, 45.89, 45.44, 45.01, 44.34, 42.06, 41.47, 39.28, 36.18, 33.86, 33.11, 32.32, 31.98, 30.73, 29.87, 27.61, 25.65, 23.75, 23.61, 23.01, 22.65, 20.40, 16.63, 15.30.

Cytotoxic analyses

Cell culture

The PC3 human prostate cancer cell lines (PC3) and the healthy human umbilical vein cell lines (HUVEC) were used in this study. The cells were cultured in Dulbecco's Modified Eagle Medium/Nutrient Mixture F-12 (DMEM-F12, Gibco, MD, USA) supplemented with 10% fetal bovine serum (FBS) and 1% penicillin/streptomycin at 5% CO_2 and 95% humidified incubator conditions.[14e,26]

MTT assay

The MTT (3-(4,5-dimethylthiazol-2-yl)-2,5-diphenyltetrazolium bromide) assay was used to determine the viability of the PC3 and the HUVEC cells. A 200 µL suspension of these cells was added to the 96-well plate (10,000 cells per well) and allowed to grow overnight. Once the cells began to grow, they were treated with the different concentrations (1, 3.125, 6.25, 12.5, 25, 50, 100, and

200 μM) of OA, target compounds (**4a–i**), and the standard drug doxorubicin for 24 h. Following treatment, MTT solution was added to each well at a final concentration of 0.1 mg/mL and then incubated for 4 h at 37 °C. After 4 h incubation of the MTT solution, the MTT reagent was removed, and DMSO was then added to each well. The mixture was further incubated for an additional 30 min at room temperature in the dark. Absorbance measurements at the 570 nm wavelength were carried out using a microplate reader (BioTek Instruments, Inc., USA). The selectivity index (SI) of each compound was calculated as the IC_{50} value in the normal cell lines (HUVEC) divided by the IC_{50} value in the cancer cell lines (PC3).[34]

Computational Studies

Protein and Ligand Preparation

The 2D structures of ligands were drawn using ChemDraw 20.1.1 and subjected to the LigPrep module of Schrodinger for energy minimization. The OPLS3e (Optimized Potential for Liquid Simulations) force field using EPIK was selected for the minimization of each structure. The 3-dimensional X-ray crystallographic structures of the target proteins were downloaded from the Protein Data Bank at the RCSB site (https://www.rcsb.org/). The three protein targets used in this study are PARP-1 (PDB ID: 5WS1, resolution of 1.90 Å), PI3K-alpha (PDB ID: 4L23, resolution of 2.50 Å), and mTOR kinase (PDB ID: 4JT5, resolution of 3.45 Å). The structures of the proteins were processed and prepared using the Protein Preparation Wizard module of Schrödinger Maestro 13.5.[35]

Induced Fit Docking (IFD)

The purpose of the induced fit docking (IFD) approach is to optimize the binding interactions between a ligand and a protein's active site by enhancing the flexibility of protein side chains. This approach allows the ligand to dynamically adjust its binding within the active site of the protein.[36] Hence, we employed IFD to examine the exceptionally dynamic interaction between ligands and proteins. The prepared ligands were docked into the receptors using the IFD protocol (Schrödinger Release 2023-1, Induced Fit Docking protocol. Glide, Schrödinger, LLC, New York, NY), which is integrated into the Schrödinger suite. The centroid of the native ligand was chosen as the center of the Glide grid. The inner box side was set to 25 Å, while the outer box side was automatically determined. The binding energy (IFD Score) was calculated for every generated pose, and the resulting poses for each protein-ligand complex were thoroughly examined visually.[36]

Prime MM/GBSA analysis

The free binding energy of the docked poses was calculated using the Prime MM/GBSA (Molecular Mechanics Generalized Born Surface Area) module of Schrödinger suite 2023 according to the method as described by Shi et al.[37] The parameters in the MM/GBSA module were set as default. Solvation model and sampling method were VSGB and Minimize, respectively. The constraints on flexible residues were used to set the residues around the receptor pocket as flexible conformation during calculation.

Molecular Dynamics Simulations

Molecular dynamic simulations for 50 ns were used to study the stability of the predicted ligand-protein complexes from the docking studies. Following the IFD experiment, the best pose of ligand-receptor complexes with the highest IFD score (**4b**, **4c**, and **4e**) were selected, and MD simulations were performed using the Desmond package of the Schrödinger Suite 2023. Using the System Builder module of the Desmond, the complex was set in a solvent-soaked orthorhombic periodic box, and a 10 Å orthorhombic box was selected as a boundary condition. The system charge was neutralized by adding Na^+ and Cl^- ions to obtain a 0.15 M NaCl salt concentration. The built solvated system was then minimized using OPLS3e. The equilibrium of the system was performed at 300 K and 1.01325 bar in the NPT (normal pressure, and temperature) ensemble. The simulations were performed for 50 ns, and data was recorded at an interval of 100 ps. Molecular dynamic trajectories were generated and analyzed using Desmond's Simulation Interaction Diagram (SID).

In silico ADME Predictions

All the synthesized compounds (**4a–i**) were analyzed with the QikProp module of Schrödinger Maestro (version 13.5; Schrödinger Release 2023-1, 2023) to predict the related ADME (absorption, distribution, metabolism, and elimination) properties. The descriptors involved in the ADME profiles of the compounds are listed in Table 3.[38]

Statistical analysis

The data was expressed as a mean ± standard error of the mean (SEM), with each experiment consisting of triplicates. Statistical differences between untreated cells and treated cells were determined using the Student's t-test. Multiple comparisons between the treatment groups were performed using ANOVA followed by Tukey's post-hoc test using GraphPad Prism 6.01.[18]

Supporting Information

NMR (^1H, ^{13}C-APT, HSQC, and ^{19}F NMR), HRMS, and FTIR spectra of all the synthesized compounds are available as supporting material. Furthermore, additional data and images of molecular docking and dynamics studies and *in vitro* biological activity plots were also given in the supporting material.

Author Contributions

Halil Şenol: conceptualized, supervised, and managed the work, managed the data and acquired the funds, molecular docking and dynamics studies, writing and reviewed the manuscript; Mansour Ghaffari-Moghaddam and Aytekin Köse: Synthesis, characterization, wrote the initial draft, and reviewed the manuscript; Şeyma Bulut and Fahri Akbaş: performed the biological activity studies and wrote the initial draft, Gülaçtı Topcu: Advised and reviewed the manuscript.

Acknowledgements

This study was financially supported by Bezmialem Vakif University (Scientific Research Project Number: 20230211). The authors would like to thank the financial support of TUBİTAK-

BİDEB 2221-Fellowships for Visiting Scientists and Scientists on Sabbatical Leave Programme.

Conflict of Interests

The authors declare no conflict of interest.

Data Availability Statement

The data that support the findings of this study are available in the supplementary material of this article.

Keywords: chalcone · in silico · oleanolic acid · prostate cancer · semi-synthesis

[1] S. Hirabayashi, Y. Li, N. Ohta, A. Ishibashi, Y. Yoshikawa, B. Lin, M. Fumimoto, T. Takehara, K. Nunomura, T. Suzuki, J. Haruta, K. Nimura, M. Arisawa, *Tetrahedron Lett.* **2023**, *114*, 154288.
[2] a) A. A. Shafi, A. E. Yen, N. L. Weigel, *Pharmacol. Ther.* **2013**, *140*, 223–238; b) R. B. Marques, N. F. Dits, S. Erkens-Schulze, W. M. van Weerden, G. Jenster, *PLoS One* **2010**, *5*, e13500.
[3] D. Poirier, R. Maltais, J. A. Rousseau, J. Roy, S. Phoenix, F. Cortés-Benítez, R. Lecomte, *Bioorg. Chem.* **2022**, *129*, 106145.
[4] W. Jiang, X. Wang, C. Shu, Q. Hou, K. Yang, X. Wu, *Bioorg. Chem.* **2022**, *119*, 105575.
[5] N. Formaggio, M. A. Rubin, J.-P. Theurillat, *Oncogene* **2021**, *40*, 1205–1216.
[6] D. Teyssonneau, H. Margot, M. Cabart, M. Anonnay, P. Sargos, N.-S. Vuong, I. Soubeyran, N. Sevenet, G. Roubaud, *J. Hematol. Oncol.* **2021**, *14*, 51.
[7] C. Thomas, Y. Ji, C. Wu, H. Datz, C. Boyle, B. MacLeod, S. Patel, M. Ampofo, M. Currie, J. Harbin, K. Pechenkina, N. Lodhi, S. J. Johnson, A. V. Tulin, *Proc. Natl. Acad. Sci. USA* **2019**, *116*, 9941–9946.
[8] S. Wang, J.-T. Shi, X.-R. Wang, H.-X. Mu, X.-T. Wang, K.-Y. Xu, Q.-S. Wang, S.-W. Chen, *Bioorg. Chem.* **2023**, *133*, 106412.
[9] M. Crumbaker, L. Khoja, A. M. Joshua, *Cancers* **2017**, *Vol. 9*.
[10] H. Wang, C. Li, X. Liu, M. Ma, *Bioorg. Med. Chem.* **2022**, *61*, 116707.
[11] C. Li, Y. Han, Z. Wang, Y. Yu, C. Wang, Z. Ren, Y. Guo, T. Zhu, X. Li, S. Dong, M. Ma, *Eur. J. Med. Chem.* **2023**, *247*, 115030.
[12] Y.-Y. Yang, W.-L. Wang, X.-T. Hu, X. Chen, Y. Ni, Y.-H. Lei, Q.-Y. Qiu, L.-Y. Tao, T.-W. Luo, N.-Y. Wang, *Bioorg. Chem.* **2023**, *132*, 106356.
[13] a) Y.-M. Kang, H.-M. Kim, M. Lee, H.-J. An, *Int. J. Mol. Sci.* **2021**, *22*, 12000; b) A. L. Xu, Y.-Y. Xue, W.-T. Tao, S.-Q. Wang, H.-Q. Xu, *Biomed. Pharmacother.* **2022**, *150*, 113007.
[14] a) S. Kumbham, M. Paul, H. Bhatt, B. Ghosh, S. Biswas, *J. Mol. Liq.* **2020**, *320*, 114389; b) H. Şenol, Ö. Özgun-Acar, A. Dağ, A. Eken, H. Güner, Z. G. Aykut, G. Topçu, A. Şen, *J. Nat. Prod.* **2023**, *86*, 103–118; c) H. Şenol, G. Çelik Turgut, A. Şen, R. Sağlamtaş, S. Tuncay, İ. Gülçin, G. Topçu, *Med. Chem. Res.* **2023**, *32*, 694–704; d) H. Şenol, B. Mercümek, R. B. Şahin, H. B. Kapucu, E. Hacıosmanoğlu, *Res. Chem.* **2022**, *4*, 100317; e) H. Şenol, K. Çokuludağ, A. S. Aktaş, S. Atasoy, A. Dağ, G. Topçu, *Org. Commun.* **2020**, *13*, 114–126; f) S. Tuncay, H. Şenol, E. M. Güler, N. Öcal, H. Seçen, A. Koçyiğit, G. Topçu, *Med. Chem.* **2018**, *14*, 617–625.
[15] J.-P. Fan, X.-H. Lai, X.-H. Zhang, L. Yang, T.-T. Yuan, H.-P. Chen, X. Liang, *J. Mol. Liq.* **2021**, *332*, 115837.
[16] F. Chu, W. Zhang, W. Guo, Z. Wang, Y. Yang, X. Zhang, K. Fang, M. Yan, P. Wang, H. Lei, *Molecules* **2018**, *23*, 322.
[17] T. I. Adelusi, A.-Q. K. Oyedele, I. D. Boyenle, A. T. Ogunlana, R. O. Adeyemi, C. D. Ukachi, M. O. Idris, O. T. Olaoba, I. O. Adedotun, O. E. Kolawole, Y. Xiaoxing, M. Abdul-Hammed, *Inf. Med. Unlocked* **2022**, *29*, 100880.
[18] F. S. Tokalı, H. Şenol, Ş. Bulut, E. Hacıosmanoğlu-Aldoğan, *J. Mol. Struct.* **2023**, *1282*, 135176.
[19] A. Pratap Singh Raman, S. Pal, P. Singh, A. Kumar, P. Jain, K. Kumari, *J. Mol. Liq.* **2023**, *381*, 121723.
[20] Z. Yang, W. Wang, Y. Qi, Y. Yang, C.-H. Chen, J.-Z. Liu, G.-X. Chu, G.-H. Bao, *Comput. Biol. Med.* **2022**, *151*, 106288.
[21] A. Rácz, L. M. Mihalovits, D. Bajusz, K. Héberger, R. A. Miranda-Quintana, *J. Chem. Inf. Model.* **2022**, *62*, 3415–3425.
[22] D. B. Warren, S. Haque, M. P. McInerney, K. M. Corbett, E. Kastrati, L. Ford, H. D. Williams, V. Jannin, H. Benameur, C. J. H. Porter, D. K. Chalmers, C. W. Pouton, *Pharm. Res.* **2021**, *38*, 1531–1547.
[23] S. A. Hollingsworth, R. O. Dror, *Neuron* **2018**, *99*, 1129–1143.
[24] J. M. Calderón-Montaño, S. M. Martínez-Sánchez, V. Jiménez-González, E. Burgos-Morón, E. Guillén-Mancina, J. J. Jiménez-Alonso, P. Díaz-Ortega, F. García, A. Aparicio, M. López-Lázaro, *Plants* **2021**, *10*, 2193.
[25] K. Singh, A. Gangrade, A. Jana, B. B. Mandal, N. Das, *ACS Omega* **2019**, *4*, 835–841.
[26] H. Şenol, A. G. Ağgül, S. Atasoy, N. U. Güzeldemirci, *J. Mol. Struct.* **2023**, *1283*, 135247.
[27] C. Yamali, H. I. Gul, M. Tugrak Sakarya, B. Nurpelin Saglik, A. Ece, G. Demirel, M. Nenni, S. Levent, A. Cihat Oner, *Bioorg. Chem.* **2022**, *124*, 105822.
[28] H. Nada, K. Lee, L. Gotina, A. N. Pae, A. Elkamhawy, *Comput. Biol. Med.* **2022**, *142*, 105217.
[29] P. S. Suresh, V. Kesarwani, S. Kumari, R. Shankar, U. Sharma, *Comput. Biol. Chem.* **2023**, *104*, 107826.
[30] L. Golea, R. Chebaki, M. Laabassi, P. Mosset, *Chem. Data Collect.* **2023**, *43*, 100977.
[31] İ. Şahin, M. Çeşme, F. B. Özgeriş, F. Tümer, *Chem.-Biol. Interact.* **2023**, *370*, 110312.
[32] H. Tijjani, A. Olatunde, A. P. Adegunloye, A. A. Ishola, *Coronavirus Drug Discovery*, Elsevier **2022**, pp. 313–333.
[33] H. Patel, R. Pawara, S. Surana, *Comput. Biol. Chem.* **2018**, *74*, 167–189.
[34] a) D. Osmaniye, Ş. Karaca, B. Kurban, M. Baysal, I. Ahmad, H. Patel, Y. Özkay, Z. Asım Kaplancıklı, *Bioorg. Chem.* **2022**, *122*, 105709; b) F. S. Tokalı, H. Şenol, T. G. Katmerlikaya, A. Dağ, K. Şendil, *J. Heterocycl. Chem.* **2023**, *60*, 645–656; c) H. Şenol, A. G. Ağgül, S. Atasoy, *Chem. Select.* **2023**, *8*, e202300481; d) H. Şenol, Z. Çağman, T. G. Katmerlikaya, F. S. Tokalı, *Chem. Biodiversity* **2023**, *20(8)*, e202300773.
[35] F. S. Tokalı, P. Taslimi, M. Sadeghi, H. Şenol, *Chem. Select.* **2023**, *8*, e202301158.
[36] P. Franco Cimino, G. María Núñez, A. Rosado-Abón, Á. Amesty, A. Estévez-Braun, K. Díaz, C. Luis Espinoza, M. A. Iglesias-Arteaga, *Steroids* **2023**, *196*, 109248.
[37] L. Shi, Z. Wen, Y. Song, J. Wang, D. Yu, *J. Mol. Graphics* **2022**, *117*, 108306.
[38] a) M. Jasani, L. Patel, *Res. Chem.* **2023**, *5*, 100739; b) S. V. Bhandari, O. G. Nagras, P. V. Kuthe, A. P. Sarkate, K. S. Waghamare, D. N. Pansare, S. Y. Chaudhari, S. N. Mawale, M. C. Belwate, *J. Mol. Struct.* **2023**, *1276*, 134747; c) B. N. Sağlık, U. A. Çevik, D. Osmaniye, S. Levent, B. K. Çavuşoğlu, Y. Demir, S. Ilgın, Y. Özkay, A. S. Koparal, Ş. Beydemir, Z. A. Kaplancıklı, *Bioorg. Chem.* **2019**, *91*, 103153.

Manuscript received: July 25, 2023
Accepted manuscript online: August 18, 2023
Version of record online: ■■, ■■